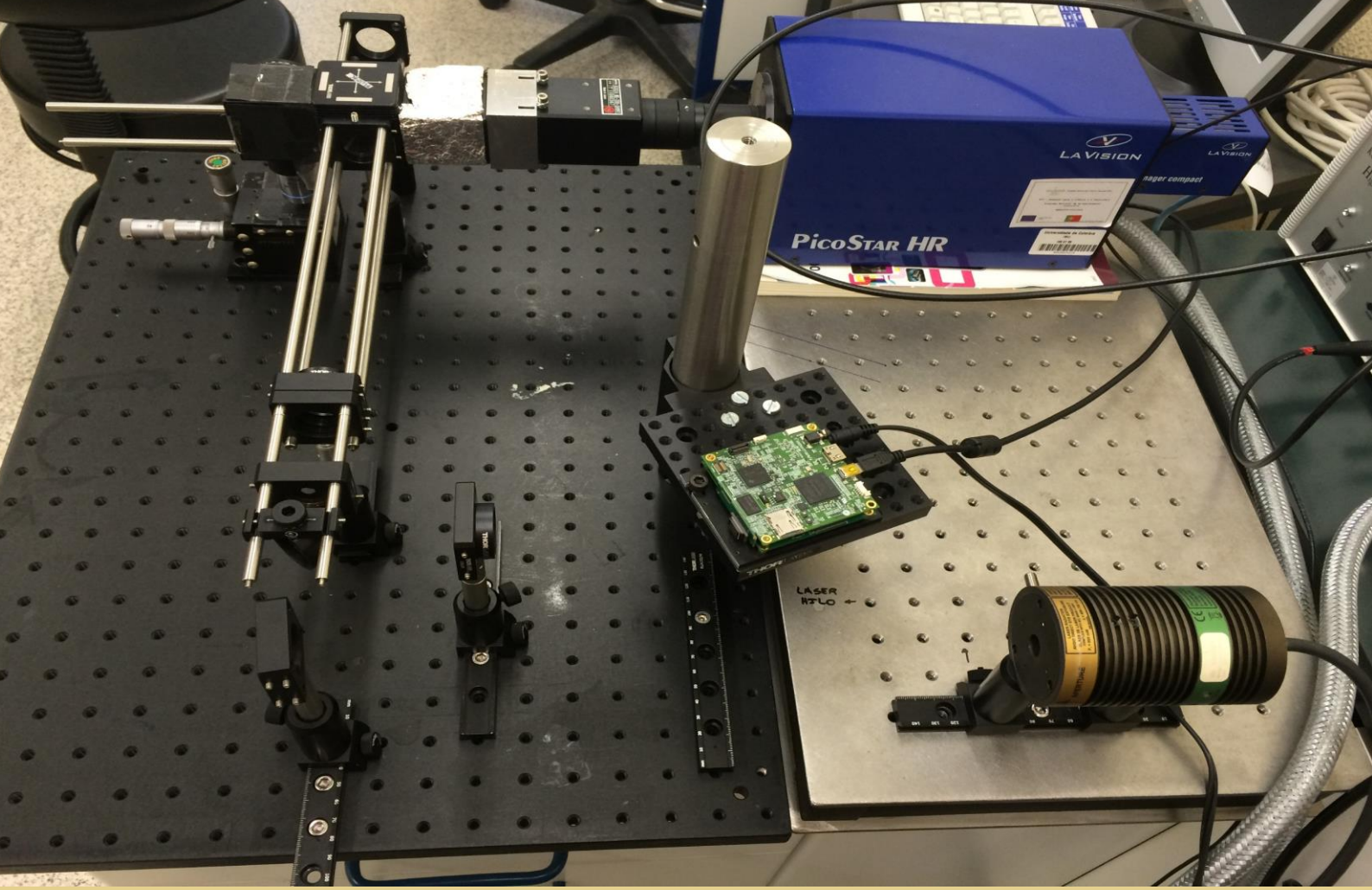

João Nuno Fernandes Jorge dos Santos Viana

Methods of optical sectioning for fluorescence lifetime imaging

Master's degree in Physics Engineering

July 2017

· U C ·

UNIVERSIDADE DE COIMBRA

UNIVERSITY OF COIMBRA
Faculty of Sciences and Technology
Department of Physics

Methods of optical sectioning for fluorescence lifetime imaging

Thesis submitted to University of Coimbra for obtaining the degree of Master in Physics Engineering

Supervised by PhD. Professor António Miguel Lino Santos Morgado

João Nuno Fernandes Jorge dos Santos Viana

Coimbra, July, 2017

ACKNOWLEDGMENTS

Firstly, I would like to thank my thesis advisor Professor António Miguel Morgado for his guidance through this project and for broadening my knowledge in many topics which was essential to finish this work.

To my lab colleague, PhD student Susana Silva who was always available whenever I needed help and was essential on the development of this work I would like to give special thanks.

To Paula, for always being there for me I thank you with all my heart.

I would like to thank my parents, brother and grandmother for all their support, my aunt and grandparents for opening their house to me during the last few years.

Finally, a thanks to all my friends who are part of my life and supported me throughout these years.

ABSTRACT

Monitoring alterations on the metabolism of corneal cells may prove to be a valuable tool for diagnosing corneal diseases prior to its pathological expression. These metabolic changes can be accessed by measuring the relative decay contributions from the autofluorescence of two metabolic co-factors, Nicotinamide Adenine Dinucleotide (NADH) and Flavin Adenine Dinucleotide (FAD).

The two co-factors exhibit double exponential decay with well-defined lifetimes. Although NADH excitation wavelength peak occurs under ultraviolet light, FAD can be excited with light on the region of the visible, making it theoretically safe for corneal imaging.

With the purpose of being able to image living cornea, a Time-Gated Fluorescence Lifetime Imaging Microscopy (TG-FLIM) with optical sectioning provided by structured illumination techniques has been built from scratch at the Institute for Biomedical Imaging and Life Sciences (IBILI) in partnership with the University of Coimbra.

This work has been mostly focused on the implementation and development of the structured illumination technique. There was a secondary task of developing a lens system to provide a small imaging magnification on the microscope.

Two optical sectioning techniques, HiLo Microscopy and Structured Illumination Microscopy (SIM) were implemented. Both techniques showed acceptable and equivalent results. However, the computing time occupied by SIM processing was much larger than the computing time by HiLo.

This project involved competences in instrumentation and data and image processing techniques, as well as knowledge on physics and optoelectronics.

RESUMO

A monitorização de alterações no metabolismo de células da córnea pode ser uma importante ferramenta no diagnóstico de doenças da córnea antes de existirem sintomas. Essas alterações podem ser observadas através da medição das contribuições relativas de decaimento provenientes da autofluoscencia de dois co-factores metabólicos, Dinucleótido de Nicotinamida e Adenina (NADH) e Dinucleótico de Flavina de Adenina (FAD)

Esses dois co-factores exibem decaimentos exponenciais duplos com tempos de vida bem definidos. Apesar do comprimento de onda correspondente ao pico de excitação do NADH se encontrar na região ultravioleta, o FAD pode ser excitado recorrendo a luz no espectro do visível, tornando a imagiologia da córnea mais segura.

Com o objetivo de estudar em tempo real uma córnea viva, um microscópio de imagiologia médica de tempos de vida de fluorescência baseado na aquisição de time-gated (TG-FLIM) com seccionamento ótico assegurado por técnicas de iluminação estruturadas foi desenvolvido no instituto biomédico de imagiologia e ciências da vida (IBILI) da Universidade de Coimbra.

Este trabalho focou-se principalmente na implementação e desenvolvimento das técnicas de iluminação estruturada. Existiu também uma tarefa secundária para fornecer uma pequena ampliação ao microscópio.

Dois métodos de seccionamento ótico, microscopia HiLo e microscopia de iluminação estruturada (SIM) foram implementadas. As duas técnicas apresentaram resultados aceitáveis e equivalentes. No entanto, o tempo de computação associado ao processamento de SIM foi muito superior ao tempo requerido pelo HiLo.

Este projeto envolveu competências em instrumentação, processamento de dados e imagens, assim como conhecimentos de física e optoelectrónica.

CONTENTS

LIST OF FIGURES

LIST OF TABLES

SIMBOLOGY

Latin upper case letters

A – Molecule at the ground state
$\boldsymbol{A^*}$ – Molecule at the excited state
D – Demodulation function
E – Energy
$\boldsymbol{I_0}$ – Fluorescence intensity immediately after the excitation pulse (equation 1.8)
$\boldsymbol{I_0}$ – Steady-state intensity (equation 1.9)
$\boldsymbol{I_1, I_2, I_3}$ – Images with pattern at the phase 0, 2π/3 and 4π/3 respectively.
I(t) – Fluorescence intensity at any given moment (equation 1.8)
I(t) – Intensity of the modulated excited light at any given moment (equation 1.9)
$\boldsymbol{I_C}$ – Widefield image
$\boldsymbol{I_{Hi}}$ – Image containing the high frequency content
$\boldsymbol{I_{HiLo}}$ – HiLo sectioned image
$\boldsymbol{I_{in}}$ – Portion of the image that is in-focus
$\boldsymbol{I_{Lo}}$ – Image containing the low frequency content
$\boldsymbol{I_{out}}$ – Portion of the image that is out-of-focus
$\boldsymbol{I_P}$ – Image intensity decay
$\boldsymbol{I_s}$ – Structured image
$\boldsymbol{I_u}$ – Uniform image
$\boldsymbol{I_{\omega E}}$ – Maximum amplitude of the signal
$\boldsymbol{J_1}$ – First order Bessel function
$\boldsymbol{K_0}$ – Cutoff frequency
$\boldsymbol{K_F}$ – Fluorescence decay rates
$\boldsymbol{K_{ic}}$ – Internal conversion transition
$\boldsymbol{K_g}$ – Spatial frequency along the x axis.
$\boldsymbol{K_{nr}}$ – Non-radiative decay rates
$\boldsymbol{K_{sc}}$ – Intersystem crossing transition
M – Contrast (equation 2.14)
M – Magnification of the objective (equation 2.20)
N(t) – Number of excited fluorophores at any given moment
NA – Numerical aperture
O – Object height
P(t) – Probability of the fluorophores decay at any given moment

$\boldsymbol{R}$ – Lateral resolution of the microscope
$\boldsymbol{S_0}$ – Electronic ground state
$\boldsymbol{S_1}$ – Electronic first excited state
$\boldsymbol{S_2}$ – Electronic second excited state
$\boldsymbol{T}$ – Transmitted light
$\boldsymbol{T_1}$ – Electronic first triplet state

Latin lower case letters

$\boldsymbol{c}$ – Speed of light
$\boldsymbol{f}$ – Focal distance
$\boldsymbol{f_g}$ – Focal distance of the lenses imaging the pattern
$\boldsymbol{f_t}$ – Focal distance of the tube lens
$\boldsymbol{f_{ob}}$ – Focal distance of the objective
$\boldsymbol{f_{eye}}$ – Focal distance of the eye piece
$\boldsymbol{h}$ – Planks constant
$\boldsymbol{m}$ – Modulation depth
$\boldsymbol{n}$ – Refractive index of the medium
$\boldsymbol{r}$ – Radius
$\boldsymbol{s}$ – Sinusoidal waveform
$\boldsymbol{u}$ – Normalized defocus along the axis
$\boldsymbol{v}$ – Spatial frequency
$\boldsymbol{v_n}$ – Normalized spatial frequency

Greek letters

$\boldsymbol{\omega_E}$ – Modulation frequency of the pulse
$\boldsymbol{\phi}$ – Phase shift
$\boldsymbol{\phi_E}$ – Initial phase shift
$\boldsymbol{\phi_0}$ – Arbitrary spatial frequency
$\boldsymbol{\theta}$ – First minimum angle
$\boldsymbol{\alpha}$ – Angular aperture of the objective
$\boldsymbol{\lambda}$ – Wavelength
$\boldsymbol{\eta}$ – Quantum efficience
$\boldsymbol{\zeta}$ – Fourier transform
$\boldsymbol{\tau}$ – Fluorescence lifetime

ABBREVIATIONS

CCD – *Charged-Coupled Device*
DMD – *Digital Micromirror Device*
FAD – *Flavin Adenine Dinucleotide*
FLIM – *Fluorescence Lifetime Imaging Microscopy*
FRET – Förster resonance energy transfer
FWHM – *Full Width at Half Maximum*
HRI – *High Rate Intensifier*
IBILI – *Institute for Biomedical Imaging and Life Sciences*
ICCD – *Intensified Charge-Coupled Device*
IRF – *Instrument Response Function*
MATLAB – *MATrix LABoratory*
MTF – *Modulation Transfer Function*
NA – *Numerical Aperture*
NADH - *Nicotinamide adenine dinucleotide hydrate*
OTF – *Optical Transfer Function*
PSF – *Point Spread Function*
PTF – *Phase Transfer Function*
SNR – *Signal-to-noise Ratio*
TAC – *Time-to-amplitude*
TCSPC – *Time-Correlated Single-Photon Counting*
TG-FLIM – *Time-Gated Fluorescence Lifetime Imaging Microscopy*
TTL – *Transistor-Transistor Logic*

INTRODUCTION

Time-Gated Fluorescence Lifetime Imaging Microscopy (TG-FLIM) is a wide-field imaging technique capable of producing a fluorescence lifetime mapping of a sample containing fluorophores by measuring the fluorescence intensity at successive delays after its excitation. The goal behind the development of this microscope is to analyse and detect metabolic alterations that may indicate a disease on the cornea.

Cornea, as the most external structure of the eye, is affected by severe pathologies that can impact deeply on the the quality of life, resulting in pain, visual impairment or even permanent vision loss. There is evidence that many of these pathologies can be diagnosed earlier by monitoring alterations in corneal cells metabolism.

The metabolic changes in cells can be accessed by the autofluorescence of two metabolic co-factors, Nicotinamide Adenine Dinucleotide (NADH) and Flavin Adenine Dinucleotide (FAD). Although both molecules exhibit double exponential fluorescence decay, with well separated lifetime components, FAD excitation wavelength peak occurs in the region of the visible, making it safer for corneal imaging, when compared with NADH imaging, which requires UV excitation. However, FAD has the disadvantage of a much lower fluorescence emission than NADH.

It is also possible to excite NADH and FAD with infra-red wavelengths, using Multiphoton Excitation. Although infra-red light is inherently safer than visible light for ocular tissue imaging, the extremely high power densities required by multiphoton absorption present a serious safety concern. So far, it was not demonstrated that Multiphoton Excitation is safe for in vivo ocular imaging

The work developed during the project associated with my master's thesis aims to optimize the performance of a Time-Gated Fluorescence Lifetime Imaging Microscope with optical sectioning based on structured illumination which was built from scratch at the Institute for Biomedical Imaging and Life Sciences (IBILI).

The first chapter introduces to the physical principles of fluorescence which constitutes the basis for fluorescence microscopy. Fluorescence lifetime microscopy will also be introduced, as well as the two domains in which FLIM can work: time and frequency domain.

On the second chapter, we will start by studying the evolution of conventional microscopy which lays the foundations on which modern day microscopy was built. Before moving on to the principles of structured illumination, there is a small introduction to confocal microscopy due to its ability to provide optical sectioning. Then, two techniques based on structured illumination are presented, structured illumination microscopy (SIM) and HiLo microscopy. To finalise the theoretical section, we will study the effect of these two techniques on the resolution of the microscope.

In the following chapter, the main components of the experimental setup of the FLIM system being developed at IBILI are presented.

The fourth chapter describes the work developed during this project. Firstly, we present the optical simulation of a Kepler telescope to be added to the microscope optical set-up. Then, the processes involved in the acquisition software are detailed, starting with the data acquisition using the software DaVis, which is also responsible for controlling multiple components of the system, including the data processing software developed in MATLAB. We will also study the process to determine the optical sectioning performance of the microscope and displaying the data.

In the final chapter, we present and discuss the results concerning the performance of the system when using the methods described in this thesis.

1. FLUORESCENCE LIFETIME IMAGING MICROSCOPY

1.1. The Basis of Fluorescence Microscopy

When a substance absorbs photons of light with enough energy, some electrons may move to electronically excited states. Their return to the ground state may occur through the emission of part of the absorbed energy. This emission of light is known as luminescence. (Lakowicz, Third Edition)

Fluorescence is a form of luminescence where the electron on the excited state is paired, with opposite spin, to the second electron which remained on the ground state. This makes the return to ground state allowed in terms of spin and thus occurring very rapidly, resulting in the emission of a photon of light with inferior energy, and thus greater wavelength, when comparing with the absorbed photon. (Lakowicz, Third Edition)

1.1.1. The principle of Florescence

Before analysing the phenomenon of fluorescence specifically, it is important to understand the photophysic processes that can occur after the absorption of light. The Jablonski diagram, shown in figure 1.1, is a representation of those processes.

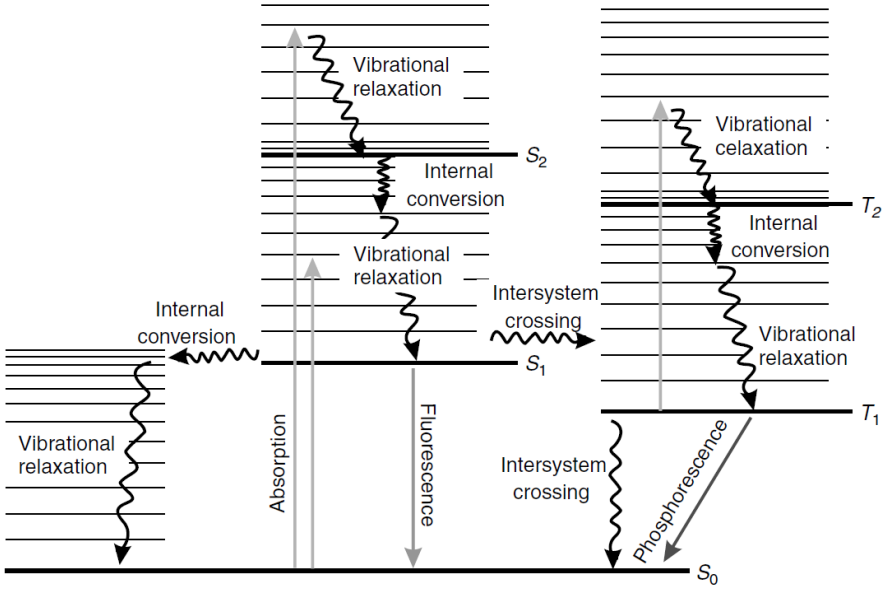

Figure 1.1 - Jablonski diagram. (Sauer, Hofkens, & Jorg, 2011)

Following excitation, the excited electron must go through internal transitions to return to the ground state, each of those transitions resulting in a loss of energy.

The Jablonski diagram contains the most common transitions which can occur on an excited molecule, namely internal conversion, vibrational relaxation, intersystem crossing, fluorescence and phosphorescence. There are also two other transitions which can be considered, although not present in the diagram, which are the delayed fluorescence and the transference of energy to another molecule. (Kubitscheck, 2013) (Marcu, French, & Elson, 2012)

In Figure 1.1, S_0, S_1 and S_2 represent the electronic states and between them there are rotational and vibrational levels. When the molecule is excited, the electron moves to a higher vibrational state of S_1 or S_2. In case it moves S_2, it will decay to S_1 through internal conversion, represented as K_{ic}. Immediately after the electron moves to a different energy level, it will vibrate and rotate in order to get to lowest vibrational level of the first excited electronic state. This process is known as vibrational relaxation. (Kubitscheck, 2013) (Marcu, French, & Elson, 2012)

The process of absorption is extremely fast, usually in the region of 10^{-15}s. Internal conversion and vibrational relaxation are in the order of 10^{-12}s.

When the electron is at lowest level of the first state it may decay to the ground state, S_0. This can happen in a radiative way, resulting in the emission of a fluorescence photon, or by a nonradiative transition, dissipating its energy as heat. (Kubitscheck, 2013) (Marcu, French, & Elson, 2012)

The two pathways are represented in equations 1.1 (radiative de-excitation of the molecule) and 1.2 (nonradiative de-excitation of the molecule), where A* represents the excited molecule and A is the molecule at the ground state. The component hv represents the energy of a photon.

$$\boldsymbol{A^* = A + hv} \quad (1.1)$$

$$\boldsymbol{A^* = A + heat} \quad (1.2)$$

The energy of the emitted photon, and thus its wavelength, will depend on the vibrational and rotational level it will decay to at the ground state. Since the energy of the photon is $E = hv$, the larger the energy gap the higher the frequency of the photon, and thus, smaller the wavelength as the wavelength is inversely proportional to the frequency per $\lambda = \frac{c}{v}$. The process of fluorescence has a time constant in the order of 10^{-6} – 10^{-9}s. (Kubitscheck, 2013)

When the electron is at the lowest electronic excited state (S_1), it can also move to the first triplet state, T_1 in a process known as intersystem crossing. This transition is regarded as forbidden since it happens between states with different spin multiplicity. For intersystem crossing to occur, the electron goes through a spin conversion before moving to T_1. It is worth mentioning that this process can happen in both directions. (Lakowicz, Third Edition)

When the electron is at the triplet state, it can decay to the ground state just as if it were in the singlet state. This phenomenon is known as phosphorescence. Although intersystem crossing is a fast process, around 10^{-12}s, phosphorescence is a much slower process than fluorescence, ranging anywhere from 10^{-3} to 10 s. Also, since the triplet state is at a lower energy when comparing to the first singlet state, phosphorescence emission usually occurs for a longer wavelength than fluorescence emission. (Kubitscheck, 2013)

As mentioned, the intersystem crossing can also be the transfer of the electron from the triplet state back to the singlet state. Then this electron can relax back to the ground state resulting in a phenomenon called delayed fluorescence.

As we have seen, due to all the internal processes following absorption, the energy of the emitted fluorescent photon is smaller than the energy of the absorbed one.

In order for fluorescence to occur, the absorbed photon must have the necessary energy to excite the molecule. Therefore, as the wavelength of light is inversely proportional to the energy, above a certain wavelength the photons can no longer cause excitation, allowing us to define a limiting wavelength at which fluorescence can still occur.

On the same line of thought, the internal processes can only cause the loss of so much energy. Therefore, it is possible to specify a range of wavelengths for the fluorescent photon. Figure 1.2 is the representation of the spectrum of fluorescein, a fluorophore present in a dye commonly used for labelling. A fluorophore is a chemical compound related with fluorescence due to its capacity to absorb light of a specific wavelength and re-emit it at a different, although also specific, wavelength.

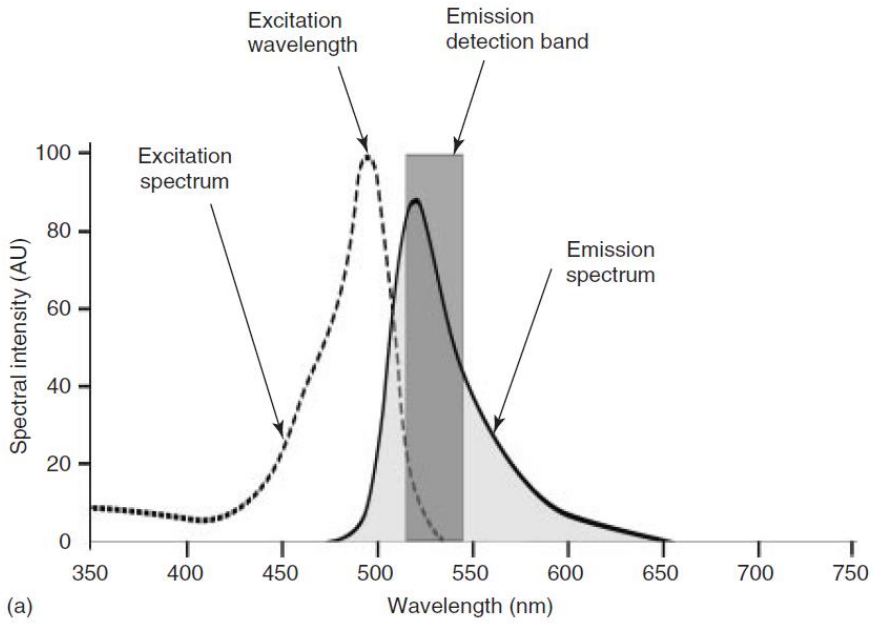

Figure 1.2 - Spectral properties of the fluorophore fluorescein. (Webb, et al., 2002)

1.1.2. Fluorescence Parameters

There are several parameters which can be helpful to quantify fluorescence.

1.1.2.1. Fluorescence Lifetime

Fluorescence lifetime τ can be described as the average time a fluorophore remains in the first excited state before returning to the ground state.

This value can be expressed as function of the fluorescence decay rate, k_f and the sum of the non-radiative decay rates, k_{nr}, which includes the intersystem crossing the and internal conversion transition rates, as represented in equation 1.3: (Marcu, French, & Elson, 2012)

$$\tau = \frac{1}{k_F + k_{nr}} = \frac{1}{k_F + k_{Ic} + k_{Isc}} \quad (1.3)$$

If we consider a single fluorophore, the decay rates should be constant. However, when a fluorophore is present in a dynamic system it is susceptible to suffer alterations that will influence the various decay rates, reflecting on the measured lifetime. The existence of FRET

or dynamic quenching can alter those values and that is why measuring the fluorescence lifetime can be used to evaluate the molecular environment of the fluorophore.

1.1.2.2. Quantum Yield

The quantum yield represents the efficiency of the fluorescence process, that is, the relation between the number of emitted fluorescence photons and absorbed photons, as represented in equation 1.4:

$$\eta = \frac{k_F}{k_F + k_{nr}} \tag{1.4}$$

where η is the quantum yield, k_F refers to the fluorescence decay rate, and k_{nr} contains the non-radiative decay pathways.

Knowing the efficiency of this process can provide information regarding the fluorophore and its environment. As mentioned earlier, the radiative decay rate can be affected by the electronic properties of the fluorophores and is, therefore, sensitive to factors that alter those distributions. On the other hand, the non-radiative decay rate can reflect changes in the local environment, specifically differences of temperature or viscosity. Nevertheless, this process is not straightforward since using the quantum yield to quantify environmental changes require previous knowledge in terms of photon excitation, detection efficiencies and fluorophore concentration and is susceptible to phenomena such as optical scattering, internal re-absorption and fluorescence backgrounds. (Marcu, French, & Elson, 2012)

1.1.2.3. Fluorophore and surrounding

A fluorophore can be classified in two distinct groups, endogenous or exogenous whether they can occur naturally in a biological system or not.

An exogenous fluorophore can be translated as “out-system”, which means it does not occur naturally in a biological system. A common example of this is fluorescein, which is usually used as a biomedical label on samples that do not display the desired spectral properties. (Marcu, French, & Elson, 2012)

Endogenous fluorophores are usually associated with the phenomenon of autofluorescence as they occur naturally. These biological molecules can be helpful since they can provide contrast between different states of tissue without the need of exogenous labels. (Marcu, French, & Elson, 2012)

There are fluorophores whose spectral properties are sensitive to a certain substance. Those fluorophores, which can be used as indicators, may reveal the present a specific substance or be used to monitor characteristics of the environment.

1.2. Fluorescence Microscopy

The first application of fluorescent material in biologic microscopy dates to the 1930s when fluorochromes were used to stain tissue components, bacteria and other pathogens. Since then, fluorescence microscopy became an essential tool on biologic and biomedical investigation with new applications of fluorescence techniques still being developed.

Fluorophores are an essential part of fluorescence microscopy. Earlier we have seen how fluorophores can be used as labels to track specific molecules or as indicators capable of revealing a specific substance due to their well-defined absorption and emission spectra.

In fluorescence microscopy, the sample is illuminated with a beam of light with a wavelength within the fluorophore absorption spectrum. Figure 1.3 represents a simplified fluorescence microscope.

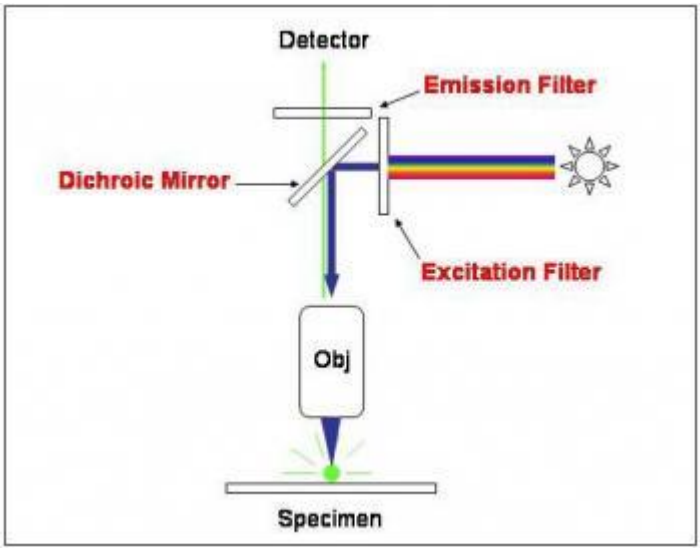

Figure 1.3 - Typical set-up of a fluorescent microscope. (Microbial Life)

In modern day fluorescence microscopy, the light source is usually implemented by a diode laser. However, other light sources can be used like xenon arc lamps or mercury vapor lamps.

An excitation filter is placed on the excitation light path to ensure that only light with the correct wavelength is projected onto the sample. A dichroic mirror is characterized by its cutoff wavelength which determines the wavelengths that are transmitted and reflected. In this type of microscopy, it is chosen a dichroic mirror where that cutoff wavelength is located between the absorption and emission wavelengths of the fluorophore, being reflective to inferior wavelengths and transmissive for superior.

The objective is essential in modern day microscopy, having the function of focusing the beam onto the sample and collect the emitted fluorescence signal. Preceding the detector is usually an emission filter. Like the excitation filter, this component ensures that only the light with the correct wavelength is transmitted to the detector.

Finally, is the detector which, as the name indicates, is responsible for detecting and recording the fluorescent signal.

1.3. Fluorescence Lifetime in Microscopy

One of the biggest drawbacks of fluorescence microscopy is the decrease of the fluorescence signal as the depth within the sample increases. Fluorescence lifetime imaging allows to overcome this difficulty, as this technique brought the capacity to reveal and quantify the presence of certain elements, even for relatively low fluorescence signals. However, in fluorescence lifetime imaging microscopy, it is not possible to possible to determine the radiative and nonradiative decay rates. Therefore, it is necessary to measure the emitted fluorescence intensity over a period of time in order to determine the lifetime of a fluorophore present in a sample. (Marcu, French, & Elson, 2012)

Following the excitation of a fluorescent sample, the number of excited fluorophores at any given moment is represented by N(t). The fluorophore decay rate from the excited state to the ground state is proportional to the number of excited fluorophores according to:

$$\frac{\boldsymbol{dN}}{\boldsymbol{dt}} = (\boldsymbol{k_F} + \boldsymbol{k_{nr}})\boldsymbol{N}(\boldsymbol{t}) \tag{1.6}$$

where t represents the time.

Since the probability of the decay of a fluorophore in a radiative way at each time instant is:

$$\boldsymbol{P}(\boldsymbol{t}) = \frac{\boldsymbol{1}}{\boldsymbol{\tau}}\boldsymbol{e}^{-\boldsymbol{t}/\boldsymbol{\tau}} \tag{1.7}$$

by combining equations 1.6 and 1.7, it is possible to express the fluorescence intensity I(t) as:

$$\boldsymbol{I(t) = I_0 e^{-t/\tau}} \quad (1.8)$$

where I_0 is the intensity immediately after the excitation pulse.

Through equation 1.8 it is possible to give a physical meaning to the fluorescence lifetime as the necessary time for the fluorescence intensity to decrease to 1/e of its initial value, as represented in Figure 1.4.

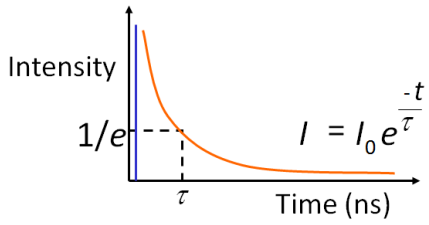

Figure 1.4 - Fluorescence intensity as a function of time. (Lambert)

In Figure 1.4, the blue line represents the excitation pulse and the red line the fluorescence emission.

1.4. Techniques of Fluorescence Lifetime Imaging Microscopy

Fluorescence lifetime imaging microscopy techniques can be classified as time-domain, where the lifetime is determined by measuring the time delay between the emission of the light pulse and the detection of the fluorescence signal, or as frequency domain if the lifetime comes from the difference of phase between the modulated excitation signal and the modulated fluorescence signal. (Marcu, French, & Elson, 2012)

The fluorescence signal detection can be performed in multiple ways, such as widefield measurements where the entire field of view is acquired at once and single point where each pixel is acquired independently from the others.

1.4.1. Frequency Domain

In order to determine the fluorescence lifetime in frequency domain, it is necessary to measure the fluorescence response of a sample to continuous intensity-modulated excitation light. Since

the fluorescence sample acts as a linear system, the fluorescence emission will mirror the modulation pattern of the excitation light, meaning there is no change in frequency. (Marcu, French, & Elson, 2012)

Although any repetitive waveform can be used, a modulated light source, usually a laser driven by a high frequency generator, is used to produce a sinusoidally modulated signal, resulting in a sinusoidally modulated radiant power. (Marcu, French, & Elson, 2012)

The intensity of the modulated excited light at each moment, I(t), can be expressed as:

$$\boldsymbol{I(t) = I_0 + I_{\omega_E} cos(\omega_E t + \phi_E)} \quad (1.9)$$

where I_0 is the steady-state intensity, $I_{\omega E}$ is the maximum amplitude of the signal, ω_E is the modulation frequency of the pulse and ϕ_E is the phase shift at t = 0.

The fluorescence emission will, as mentioned, mirror the sinusoidal pattern of the excitation light. However, this fluorescence signal will also reflect the lifetime of the fluorescent process in the form of a phase delay, ϕ, and a decrease in modulation depth, M, as represented in Figure 1.5.

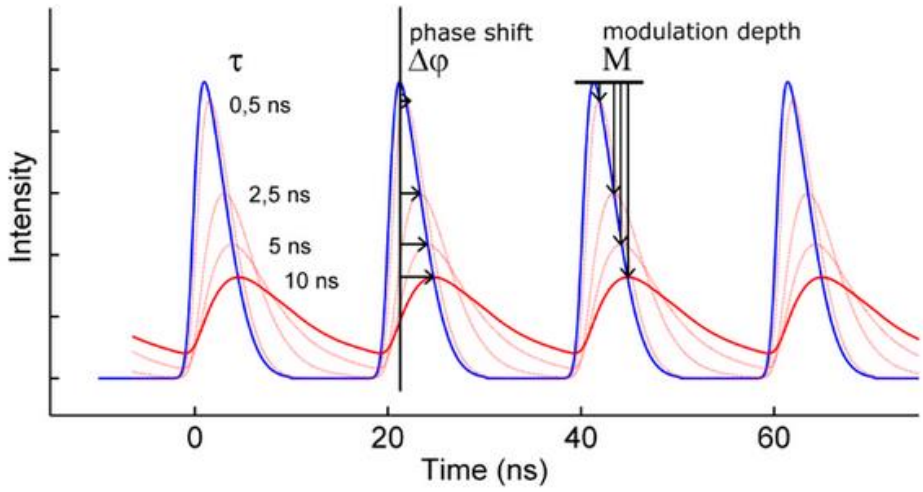

Figure 1.5 - Fluorescence response for different lifetimes to a series of pulses in frequency domain. (Lambert)

Figure 1.5 shows the influence of the samples lifetime on the phase shift and modulation depth of the fluorescence signal. As seen, for longer lifetimes the phase shift will increase while the amplitude of the fluorescence signal decreases.
Both constants are a function of the modulation frequency of the excitation pulse and the fluorophore lifetime according to:

$$\tan(\phi) = \omega\tau \tag{1.10}$$

$$m = \frac{1}{\sqrt{1 + \omega^2\tau^2}} \tag{1.11}$$

The decrease in modulation depth, m, can also be referred to as a modulation ratio.

1.4.2. Time Domain

Time-Domain FLIM is based on the temporal response of a fluorophore to a single light pulse. When a high frequency laser is used to produce a train of ultrashort pulses, it will result in a sequence of fluorescence signals as represented in figure 1.6.

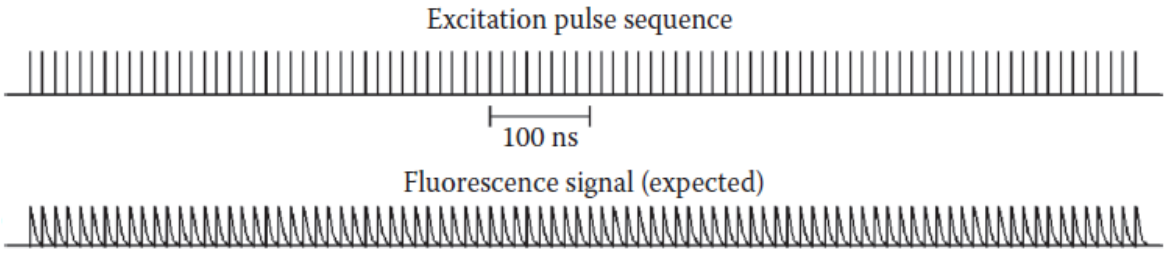

Figure 1.6 - Excitation pulse sequence and respective expected fluorescence waveform. (Marcu, French, & Elson, 2012)

In most FLIM measurements, the fluorescence signal will be acquired by a bi-dimensional detector, commonly a charge-coupled device (CCD) camera. The expected lifetime of most biological samples is on the order of hundreds of picoseconds to a few nanoseconds. It is necessary that this lifetime fits inside each pulse period. So the repetition rate of the laser is usually between 10-100MHz. Currently, the available CCD cameras have a photon detection rate around 10kHz-1MHz, making impossible to process every cycle of the fluorescence process represented in figure 1.7. Instead they collect several cycles to create a lifetime map.

The detected signal would look somewhat similar to figure 1.7, which represents an oscilloscope trace of such a fluorescence signal. (Marcu, French, & Elson, 2012)

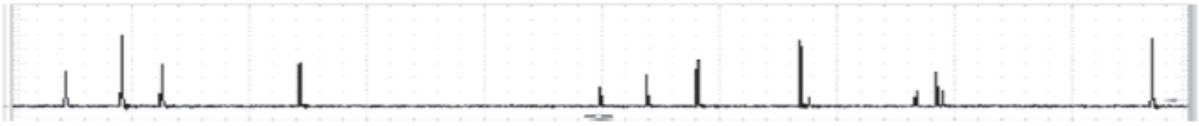

Figure 1.7 - Time trace of the fluorescence signal detected by a detector. (Marcu, French, & Elson, 2012)

Two techniques with very different approaches are currently used to determine the fluorescence lifetime of a sample in time-domain: a single-point scanning technique called Time-Correlated Single-Photon Counting (TCSPC) and a widefield technique known as Time-Gated. (Marcu, French, & Elson, 2012)

1.4.2.1. Time-Correlated Single-Photon Counting

TCSPC is a technique where the sample is sequentially scanned, i.e., each point of the sample is separately scanned by focusing the beam of a high-frequency pulsed laser. Data recording is based on the detection of single photons and their timing, through the measurement of their arrival time. The acquired data is then used to create a histogram for each point containing the recorded arrival times, which, in adequate experimental conditions, corresponds to the decay profile of the fluorescent signal. This process is depicted in figure 1.8. (Marcu, French, & Elson, 2012)

As seen, in any time-domain technique a high frequency laser is used to create a train of pulses. At each pulse, the laser source sends a trigger signal to the detector marking the beginning of each cycle. In TCSPC, when a pixel detects a photon, it initiates a time-to-amplitude (TAC) conversion resulting in a voltage signal. The gain of the TAC increases proportionally with time, and is only restored at the end of each cycle. This way, the amplitude of the output signal will be proportional to the photon arrival time, thus the time spent in the excited state. (Marcu, French, & Elson, 2012)

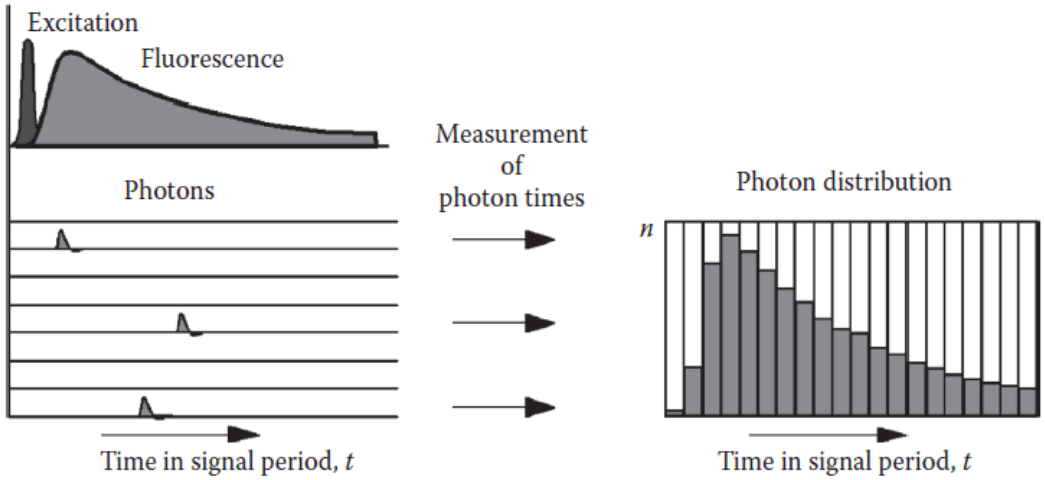

Figure 1.8 - Histogram of single-photon arrival times in TCSPC. (Marcu, French, & Elson, 2012)

Due to the high repetition rate of the laser, the light pulses are ultra-short, meaning the probability of detecting a photon is significantly lower than one. This leads to two important features of TCSPC. Firstly, when multiple photons reach the position of the detector, only the first photon is time, i.e. its arrival time is recorded.

When a photon is detected, the event is recorded in memory by adding a '1' in a memory location with an address proportional to the arrival time. This leads to the other important feature of TCSPC: when no photon is timed, it does not register any information, resulting in an improvement of the signal-to-noise ratio (SNR). (Marcu, French, & Elson, 2012)

When enough signals have been detected for the individual point being scanned, the laser is refocused to the next position and the recorded delay times are used to build a histogram as shown in Figure 1.8. That histogram is a reproduction of the illumination profile, and thus of the samples fluorescence decay.

This technique has other important features concerning lifetime imaging, as it can resolve complex decay profiles, is tolerant to dynamic changes in the fluorescent decay parameters during acquisition and is compatible with other types of laser scanning systems such as confocal and multiphoton microscopy.

1.4.2.2. Time-Gated

Time-Gated FLIM is an acquisition method which, similarly to TCSPC, works in time domain. However, these two techniques have two important differences in terms of acquiring and processing the sample.

Firstly, TCSPC is a point scanning technique while in TG-FLIM the whole sample is illuminated and acquired at once. The most important difference is related to lifetime mapping reconstruction. TCSPS uses a statistical approach by building a histogram to determine the fluorescence lifetimes of the sample, while on TF-FLIM the decay curve is directly sample through the acquisition of multiple images.

Both methods use a pulsed laser as light source, which will be connected to a module responsible for sending a trigger to the acquisition system. Following the trigger, the detector will acquire the whole field of view during a pre-specified time interval (gate width) place at a pre-specified delay. To create a fluorescence lifetime map, a set of short gated intensity images is acquired at increasing delays following the excitation pulse. This technique is represented in figure 1.9. (Dupuis, Benabdallaha, Chopinauda, Mayeta, & Lévêque-Fort, 2013)

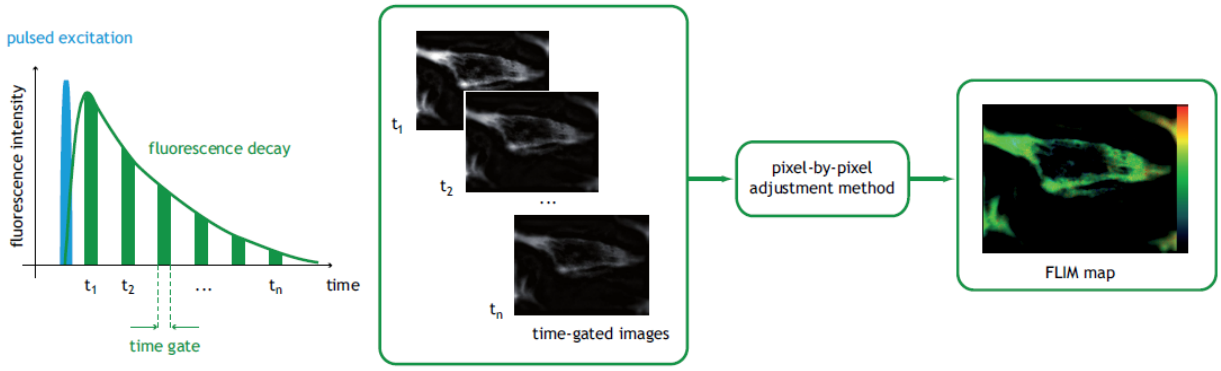

Figure 1.9 - Principle of time-gated FLIM. (Dupuis, Benabdallaha, Chopinauda, Mayeta, & Lévêque-Fort, 2013)

The first difficulty of this technique is the acquisition hardware. The acquisition of a single intensity fluorescence image requires a bi-dimensional detector, usually a CCD camera. However, when we consider the need of acquiring a set of sequential images it is necessary to introduce an ultra-fast shutter capable of gating images in the nanosecond range. As this cannot be accomplished mechanically, an optical image intensifier with electronically modulated gain and high repetition rate is the most common choice. The working principle of a CCD camera

and an intensifier will be presented with more detail on the next chapter. (Marcu, French, & Elson, 2012)

With an adequate number of acquired images it is possible to create a fluorescence lifetime time map as shown in Figure 1.9. Although this process requires advanced processing techniques, nowadays there are several software programs capable of calculating and creating the fluorescence lifetime map in a question of minutes with a reduced number of images. When the resulting data is well detailed it can be used to create a multi-exponential lifetime fitting and determine the various lifetimes presented in a sample.

2. OPTICAL SECTIONING IN MICROSCOPY

Optical sectioning can be described as the ability to extract only a section of the sample while rejecting the rest of the information, known as out-of-focus. The strength of a microscope's optical sectioning can be measured in terms of its spatial resolution.

As we have seen in the previous chapter, conventional fluorescence widefield microscopy brings many new possibilities in several fields such as disease diagnosis. However, by itself it does not possess the ability to provide an image with depth resolution. To solve this issue, there were invented ways of extracting that information and create a corresponding image with that information. (Marcu, French, & Elson, 2012)

In this chapter, we will start by focusing on the limits of conventional widefield microscope and give a small introduction to confocal microscopy as one of the best methods of achieving optical sectioning. Following, we will study two optical sectioning techniques which apply the principles of structured illumination and see their impact on the microscopes resolution.

2.1. The limits of conventional widefield microscopy

The invention of the first optical microscope is attributed to Robert Hooke in the 17th century. His microscope however, had many limitations, being the quality of the lenses the most significant. Nevertheless, during that period it was already possible to reach over 200x magnifications using a single movable lens as an objective capable of focusing the sample. (Kubitscheck, 2013)

Since the 19th century, microscopy has been an important subject for scientists around the world. Multiple breakthroughs were made, being the first significant one in 1835, when George Airy could explain theoretically the effect resulting from the passage of light through an aperture.

The projection of a point source of light from an object through an ideal lens should form a perfectly scaled replica of the object. However, it is not realistic to expect this to happen in a system containing a lens and an aperture. That is due to factors related to the lenses used, such as aberration and to the diffraction of light.

In a real system, the object forms a blurred and scaled replica itself. Considering the object as a point source, the resulting image is a series of concentric rings known as the Airy disks as shown in Figure 2.1.

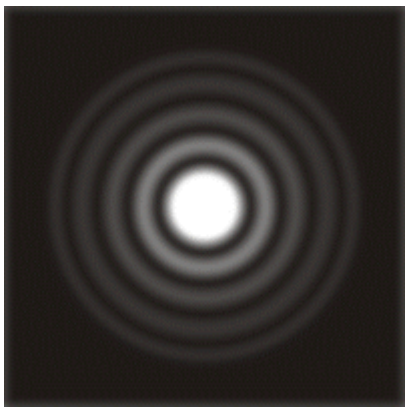

Figure 2.1 - Airy disks. (Telescope Equations)

Spatial resolution is an important concept in microscopy, as it is a measure of the resolving power of a microscope. It can be described as the smallest distance between two objects that can be seen separately, or the smallest distance which allows to distinctly distinguish two point sources.

As the objects get closer, their Airy disks start to superimpose making the job of distinguishing them harder. This phenomenon is represented in Figure 2.2.

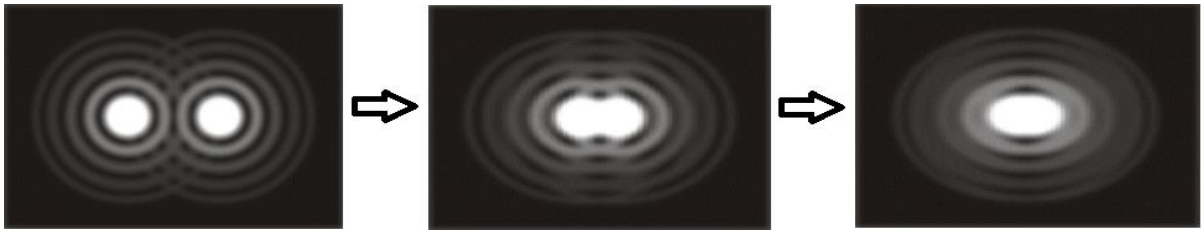

Figure 2.2 - Airy disks of two close objects. (Telescope Equations)

The minimum distance at which is still possible to distinguish the two objects can be expressed as the radius of the Airy disk, i.e., the region enclosed by the first minimum of the Airy pattern and containing 84% of the radiant energy. (Microscopy Resource Center)

In 1874, Ernst Abbe, after expanding Airy's theory, was able to relate the size of the disks, and thus the resolution of the microscope, with two characteristics of the setup, the numerical aperture of the objective (NA) and the wavelength of the light source, according to: (Kubitscheck, 2013). The NA is defined as

$$\boldsymbol{NA = 2n\,sin(\alpha)} \tag{2.1}$$

where n is the refractive index of the surrounding medium and α is the angular aperture of the objective.

The lateral resolution of the microscope can then be written as

$$\boldsymbol{R = \frac{\lambda}{2\,NA}} \tag{2.2}$$

where λ is the wavelength and NA is the numerical aperture.

Since the resolution is written as a function of distance, from equation 2.2 it is possible to calculate a limiting spatial frequency, or cutoff frequency, which can be projected onto an image and still be detected.

$$\boldsymbol{k_0 = \frac{2\,NA}{\lambda}} \tag{2.3}$$

From equation 2.3 it is possible to conclude that the resolution in a microscope increases with larger numerical apertures and shorter wavelengths.

The Point Spread function (PSF), represented in Figure 2.3, is a graphic representation of the normalized contrast of an Airy disk.

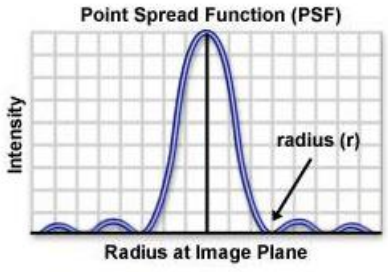

Figure 2.3 - Point Spread Function of an Airy disk. (Moleculcar Expressions)

The Rayleigh two-point criterion is an optical indicator which uses the width distribution of the PSF to determine the resolution. For a lens with a circular aperture, the first minimum in the diffraction pattern occurs at

$$\boldsymbol{\theta = 1.22 \frac{\lambda}{NA}} \tag{2.4}$$

In the 19th century, Lord Rayleigh was able to determine, based on the angle of the first minimum, the currently accepted criterion for the resolution limit of a microscope:

$$\boldsymbol{R = 0.61 \frac{\lambda}{NA}} \tag{2.5}$$

The system response to a point source can also be expressed in the frequency domain, in the form of the modulation transfer function (MTF), a normalized contrast function of spatial frequency which express the capacity of the system to transfer contrast. (Microscopy Resource Center)

The MTF is derived from the PSF using the Fourier transform per:

$$\boldsymbol{MTF = \zeta(PSF)} \tag{2.6}$$

where ζ is the Fourier transform of the PSF.

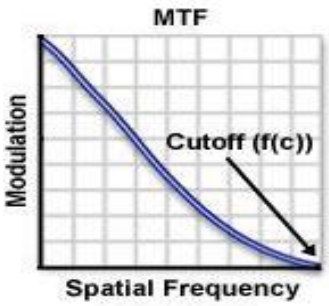

Figure 2.4 - Modulation Transfer Function of a point spread function. (Moleculcar Expressions)

Having the graphic representation of the MTF also allows to determine the limiting spatial frequency.

The phase shift between the object and the image is taken into consideration through the phase transfer function (PTF), it is possible to obtain the optical transfer function (OTF) of the system, per:

$$\boldsymbol{OTF = MTF * e^{i\Phi(v)}} \quad (2.7)$$

where $e^{i\Phi(f)}$ represents the PTF of the system, Φ is the phase at the spatial frequency v.
It is possible to observe from the previous equation that the optical transfer function is a complex function where the amplitude is the modulation transfer function and the phase comes from the phase transfer function.

2.2. Confocal microscopy

Optical microscopy has come a long way since its invention. As we have seen in the previous chapters, the 19th brought many changes and opened new possibilities.

However, when we consider conventional microscopy, it has some crucial limitations. Firstly, while the lateral resolution is defined by the Rayleigh limit, it does not provide optical sectioning. Also, when we consider fluorescence microscopy of thicker specimens, the fluorescence emission is so high that a lot of details are lost. (Microscopy Resource Center)

The concept of the confocal microscope was initially developed by Marvin Minsky in the 1950s. Nowadays, due to its capacity of controlling the field depth, eliminating most of the out of focus portions and acquiring a series of optical sections while providing high quality image it is one of the most used techniques on the biologic study of fixed and living cells. (Microscopy Resource Center)

The confocal microscope brought a new scanning technique. In opposition to widefield, where the whole sample is illuminated at once, in this technique the sample was to be scanned point by point, i.e., a series of sequential images is collected from the section of the specimen. (Kubitscheck, 2013)

To create a confocal microscope, the excitation light and the detector have to be in focus. This process is accomplished by implementing two pinholes in the two confocal points of the section of the sample being imaged. The first one is placed following the light source while the second, being responsible for the elimination of the majority of the out-of-focus rays is placed before the detector. (Microscopy Resource Center)

This process is exemplified in Figure 2.5 where the optical configuration of a laser scanning confocal microscope is presented.

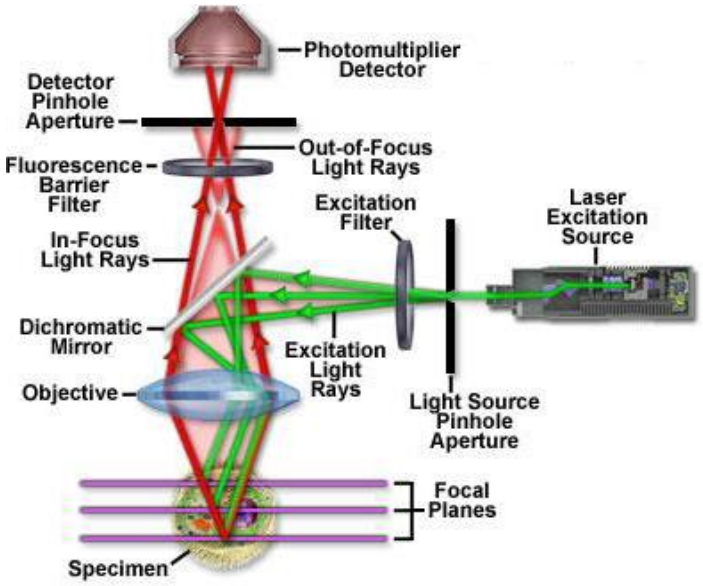

Figure 2.5 - Setup of a laser scanning confocal microscope. (Microscopy Resource Center)

As mentioned, the point scanning microscope performs point to point scanning. Therefore, the excitation light has to focus onto the target section of the sample. To reduce the volume of the light cone leaving the objective, the beam is expanded to fill its rear aperture and focused to a small spot at the focal plane. (Microscopy Resource Center)

This technique reduces greatly the amount of background emission from the sample improving the contrast and the resolution of the microscope. Figure 2.6 exemplifies this process.

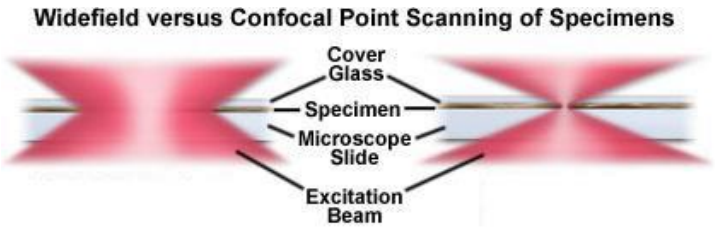

Figure 2.6 - Light focus on widefield conventional microscopy against confocal microscopy. (Microscopy Resource Center)

In terms of results, confocal microscopy can produce thin optical sections, in the region of a few micrometres. In terms of contrast and image quality it can achieve much better results than conventional widefield due to reduction of out of focus contributions and consequent improvement of signal to noise ratio. (Microscopy Resource Center)

Concerning the lateral resolution, the performance is similar to conventional microscopy.

2.3. The principle of structured Illumination

Structured illumination presents an innovative way of providing depth resolution to widefield fluorescence microscopy while producing high quality images with good contrast.

Confocal point scanning optical microscopy is a good example of a system with a coherent image formation. In a coherent image formation, all spatial frequencies within the optical transfer function attenuate with defocus. On the other hand, in widefield microscopy, image formation is only partially coherent, which means that not all spatial frequencies will attenuate with defocus. (Neil, Juskaitis, & Wilson, 1997)

After analysing the optical transfer function of the system, it was found that only the zero-spatial frequency does not attenuate with defocus. This zero frequency represents the d.c. component and typically it blurs the image and degrades the sectioning. (Neil, Juskaitis, & Wilson, 1997)

By projecting a single spatial frequency grid pattern into the sample, it is possible to produce a spatially modulated excitation and resulting fluorescence distribution. The pattern will only be efficiently imaged in the portion of the object that is in focus. There may be some residual pattern on some of the out-focus portion closer to the imaged section, but these residues will be blurred and have lower contrast in comparison with the in-focus strips, making it theoretically possible to digitally distinguishing them. (Neil, Juskaitis, & Wilson, 1997)

The creation of the pattern is achieved either by placing a physical grid in the excitation light path or digitally using a special light modulator such as a programable liquid crystal or a digital micromirror device (DMD). (Heintzmann, 2006)

Figure 2.7 exemplifies a possible setup for a wide-field microscope with structured illumination. In this example, a physical grid is being used to produce the pattern and the detection is carried-out with a charge-coupled device (CCD) camera.

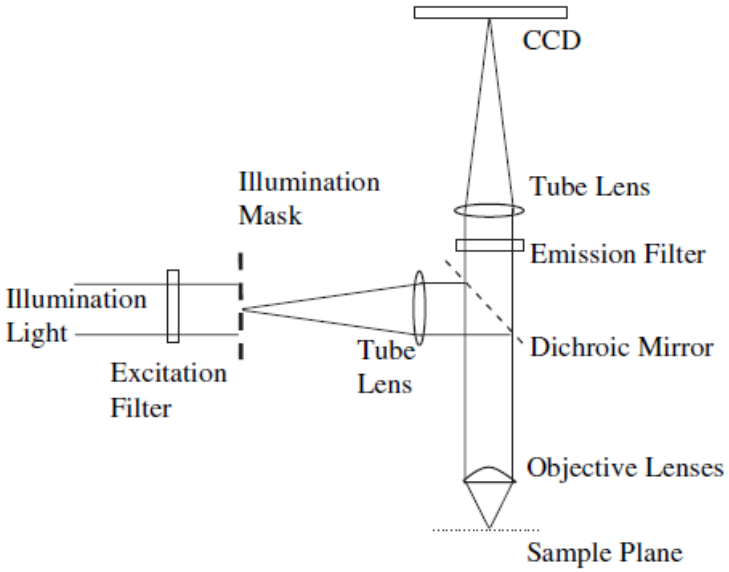

Figure 2.7 - Generic setup of a structured illumination microscope. (Heintzmann, 2006)

The grid pattern will create a mask with the form of a square wave. However, due to diffraction of light on the multiple lenses, the objective of the microscope and the finite bandwidth of the optics, the mask will in fact present a form close to a sinusoidal wave, as represented in equation 2.8.

$$\boldsymbol{s(x,y) = 1 + m\cos(2\pi vx + \Phi_0)} \qquad (2.8)$$

where m is the modulation depth, v is the spatial frequency and Φ_0 is an arbitrary spatial phase.

This effect was mentioned earlier in the form of the modulation transfer function and the phase transfer function of a system and is represented in Figure 2.8. As we can see, increasing the frequency of the pattern will reduce the contrast of the grid projected onto the sample.

This represents one of the difficulties of choosing the grid, because higher frequencies are preferable for this method but it is necessary to obtain acceptable contrast.

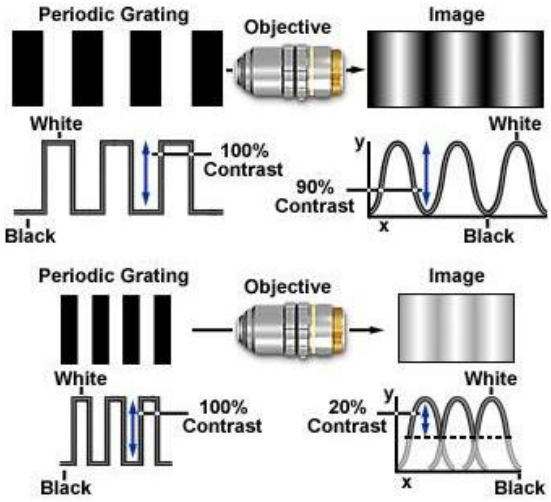

Figure 2.8 - Transfer of contrast for different grid frequencies. (Microscopy U)

Assuming an ideal system where the pattern is only projected onto the in-focus portion, it is possible to divide the acquired image by the detector in two parts, per

$$\boldsymbol{I(x,y) = I_c + I_s \cos(2\pi v x + \Phi_0)} \qquad (2.9)$$

The first part of the equation, I_c, is the portion of the image without the pattern and represents what would be acquired with conventional widefield microscope. The second part is the in focus section. However, this portion has the projected pattern superimposed. In the following section two methods will be presented in order to isolate I_s and removing the pattern. (Webb, et al., 2002)

2.4. Optical Sectioning Structured Illumination Microscopy

In this chapter, we will study two techniques which apply the principles of structured illumination capable of removing the projected pattern which will be used throughout the practical part of this thesis.

The first method studied is simply known as structured illumination microscopy (SIM) as it was the original technique to which structured illumination was developed. The second method uses the same basis but the creation of an optically sectioned image is made by manipulating the Hi and Low frequencies of the images.

At this moment, only the theoretic approaches behind each method will be considered. In reality, the images require further image processing which will be addressed later.

2.4.1. Structured Illumination Microscopy

This innovative approach to remove the unwanted pattern was introduced by M. A. A. Neil, R. Juskaitis and T. Wilson in 1997 and has proven to be extremely effective in removing the grid pattern with minimal effect in the quality of the image. (Neil, Juskaitis, & Wilson, 1997)

This technique works by acquiring three consecutive images (I_1, I_2 and I_3) and eventually conjugate that information in one single image containing the in focus information whilst eliminating the pattern and the out focus porting of the image. In each of the acquired image a sinusoidal pattern is projected onto the sample, with the same fundamental frequency but with a relative phase shift of 2π/3. The pattern in the first image is considered as being the phase 0, being the other two images at 2π/3 and 4π/3.

The optically sectioned image can be obtained by applying the algorithm presented in equation 2.10 and the conventional image is the average of the three acquired images, as represented in equation 2.11.

$$\boldsymbol{I_s = \frac{3}{\sqrt{2}}[(I_1 - I_2)^2 + (I_1 - I_3)^2 + (I_2 - I_3)^2]^{1/2}} \quad (2.10)$$

$$\boldsymbol{I_c = \frac{I_1 + I_2 + I_3}{3}} \quad (2.11)$$

By analysing equation 2.10, it is easy to understand its fundaments. Since the sinusoidal pattern will only be projected onto the in focus planes, the three images acquired should have the same intensity in the out-of-focus planes. If this condition is verified, the obtained structured image will eliminate the entire out-of-focus component.

The calculation of the sectioned image involves the three images so if the stripes are well defined, applying this method should be capable of removing the pattern. However, there are a lot of factors that can affect this process, such as inaccurate phase shifting or lack of contrast to determine the in focus section. This technique is also vulnerable to the relative noise level and the dynamic range of the camera (Webb, et al., 2002)

2.4.2. HiLo Microscopy

HiLo microscopy was introduced by Daryl Lim, Kengyeh Chu and Jerome Mertz in 2008. In terms of image acquisition, this technique only requires two images, instead of the three associated with SIM. However, just one of the images has the pattern projected onto the sample, being the other a regular widefield image. (Bhattacharya, et al., 2012)

The two images will then be combined to form a reconstructed image where the in-focus high frequency content (Hi) is extracted from the uniform image while the low frequency (Lo) is obtained from the image with the grid pattern. The Hi and Lo contents are then combined using a scaling factor to ensure a smooth transition between images. (Bhattacharya, et al., 2012)

The uniform image, designed as I_u, is a simple wide-field image and carries the in-focus information (I_{in}), which we will try to isolate, as well as the out-of-focus background (I_{out}).

$$\boldsymbol{I_u(\vec{p}) = I_{in}(\vec{p}) + I_{out}(\vec{p})} \tag{2.12}$$

where $\vec{p}$={x,y} represent the spatial coordinates of the image plane.

In a similar way, the non-uniform image can be decomposed into:

$$\boldsymbol{I_n(\vec{p}) = \frac{1}{2}[I_{in}(\vec{p})(1 + M\,sin(k_g x) + I_{out}(\vec{p})]} \tag{2.13}$$

where M represents the contrast and k_g the spatial frequency in the x axis. The factor ½ is a rough approximation of the effect of the grid in the total power on the non-uniform image, in comparison with the uniform image. (Mertz & Kim, January/February 2010)

The exact portion of light that is transmitted using a square grating can be expressed per:

$$\boldsymbol{T = \frac{1}{2} + \frac{2}{\pi}(cos(2\pi\upsilon x + \phi_0) - \frac{1}{3}(3cos(2\pi\upsilon x + \phi_0) + \frac{1}{5}(5cos(2\pi\upsilon x + \phi_0) - \cdots} \tag{2.14}$$

where T represents the transmitted light, υ is the grating period and ϕ_0 is an arbitrary phase. (Marcu, French, & Elson, 2012)

In I_n, the low spatial frequencies of the in-focus contribution are modulated, whereas the low spatial frequencies of the out-of-focus contribution are not. The low spatial frequencies of the focal plane can be extracted via the demodulation function expressed in equation 2.15.

$$\boldsymbol{D(\vec{p}) = |HP[I_u(\vec{p}) - 2I_n(\vec{p})]| = I_{in}(\vec{p})M\,sin(k_g x)} \quad (2.15)$$

The applied high pass filter (HP), with a low cutoff frequency so that no important information is eliminated, ensures that I_u - $2I_n$ is centred around zero. (Schaefer, Schaefer, & Schuster, 2004)

The low content, I_{lo}, is then obtained by applying a low pass filter (LP) to the demodulation function. The cutoff frequency of this filter is slightly lower than the spatial frequency k_g of the pattern.

$$\boldsymbol{I_{Lo}(\vec{p}) = LP[D(\vec{p})]} \quad (2.16)$$

By definition, out-of-focus contributions exhibit only low frequency spatial structure. Therefore, the high spatial frequencies present in the uniform image necessarily come from the in-focus contribution. To obtain the high frequency content, a complementary high pass filter with the same cutoff frequency is then applied to the uniform image. (Mertz & Kim, January/February 2010)

$$\boldsymbol{I_{Hi}(\vec{p}) = HP[I_u(\vec{p})]} \quad (2.17)$$

Finally, in order to achieve an optically sectioned image of the desired depth, the two obtained images, that is, the Hi and Lo components are combined.

$$\boldsymbol{I_{HiLo}(\vec{p}) = \eta I_{Lo}(\vec{p}) + I_{Hi}(\vec{p})} \quad (2.18)$$

where the factor η is a scaling factor that ensures a seamless transition from low to high frequencies in I_{HiLo}.

The pocesses described are simplified in Figure 2.9.

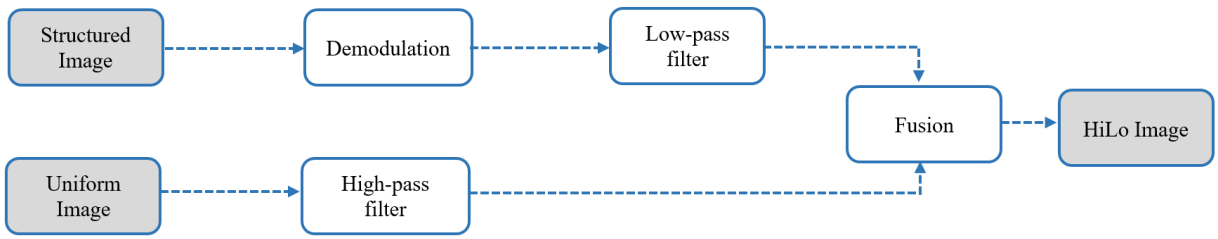

Figure 2.9 - Representation of HiLo microscopy pos-processing.

2.5. Limits of resolution with structured illumination

As a reminder, in conventional widefield microscopy, the lateral resolution of the microscope was defined by the numerical aperture of the objective and the wavelength of the light.
After explaining the principle behind SIM and its two most common methods it is time to study the theoretical result in terms of resolution.

The main goal of structured illumination is the ability to achieve optical sectioning, i.e., improving the axial resolution. Despite the existence of other techniques which apply the principles of structured illumination that may increase the lateral resolution, the two methods studied do not provide any significant improvement in that chapter, meaning that resolution is still determined by the classical approach of the Rayleigh criterion. (Webb, et al., 2002)

The optical sectioning strength is defined as the axial distance between two point at which the intensity of the sectioned image has half the value of that when the grating is in focus. (Webb, et al., 2002)

This definition allows to determine the theoretical normalized axial resolution from the image intensity decay, I_p, and the normalized spatial frequency, v_n, per:

$$\boldsymbol{I_p(z) = \left| \frac{2J_1\left[u * v_n * \left(1 - \frac{v_n}{2}\right)\right]}{\left[u * v_n * \left(1 - \frac{v_n}{2}\right)\right]} \right|} \tag{2.19}$$

where J_1 is the first order Bessel function.

$$\boldsymbol{v_n = \frac{f_g * \lambda * M * v}{(NA) * f_t}} \tag{2.20}$$

where f_g and f_t are, respectively, the focal distances of the lenses imaging the grating and the tube lens, λ is the wavelength, M is the magnification of the objective, v is the frequency of the grid used to generate the pattern and NA is the numerical aperture.

The parameter u represents the normalized defocus along z.

$$\boldsymbol{u = \frac{8\pi}{\lambda} * z * n * \sin^2\left(\frac{\sin^{-1}\left(\frac{NA}{n}\right)}{2}\right)} \tag{2.21}$$

Later in this thesis, there will be a comparison between the theoretical optical sectioning and the results obtained using the detailed methods.

3. THE FLUORESCENCE LIFETIME IMAGING MICROSCOPE

3.1. Working Principle

The microscope system is based in a Time-Gated detection setup. In terms of the illumination elements, a pulsed diode laser acts as source of light, a digital micromirror device (DMD) is responsible for producing the pattern for structured illumination, a Keplerian telescope provides the necessary magnification to the laser beam and a positive lens converts the collimated rays into converging rays onto the conjugate plane of the objective. A dichroic mirror is used to separate the excitation wave from fluorescence. The objective will transmit the excitation light onto the sample and collect the fluorescence signal. The tube lens is positioned between the objective and the detection system to form the image onto the primary image plane of the camera. Finally, a high rate intensifier (HRI) and a Charged-coupled Device (CCD) camera are responsible for acquiring the fluorescence signal.

Figure 3.1 is the schematic of the microscope using a DMD to produce the pattern, while Figure 3.2 is an alternative set-up replacing the DMD with a physical grid.

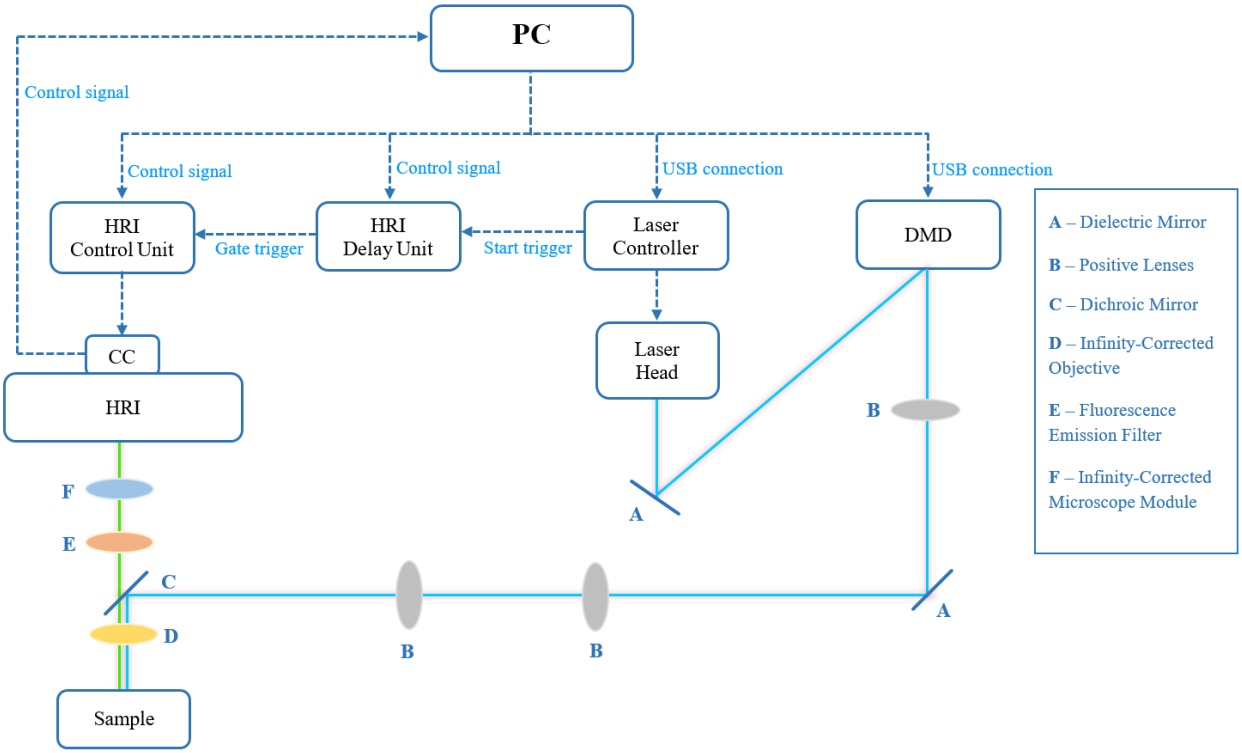

Figure 3.1 - Microscope Setup using the DMD.

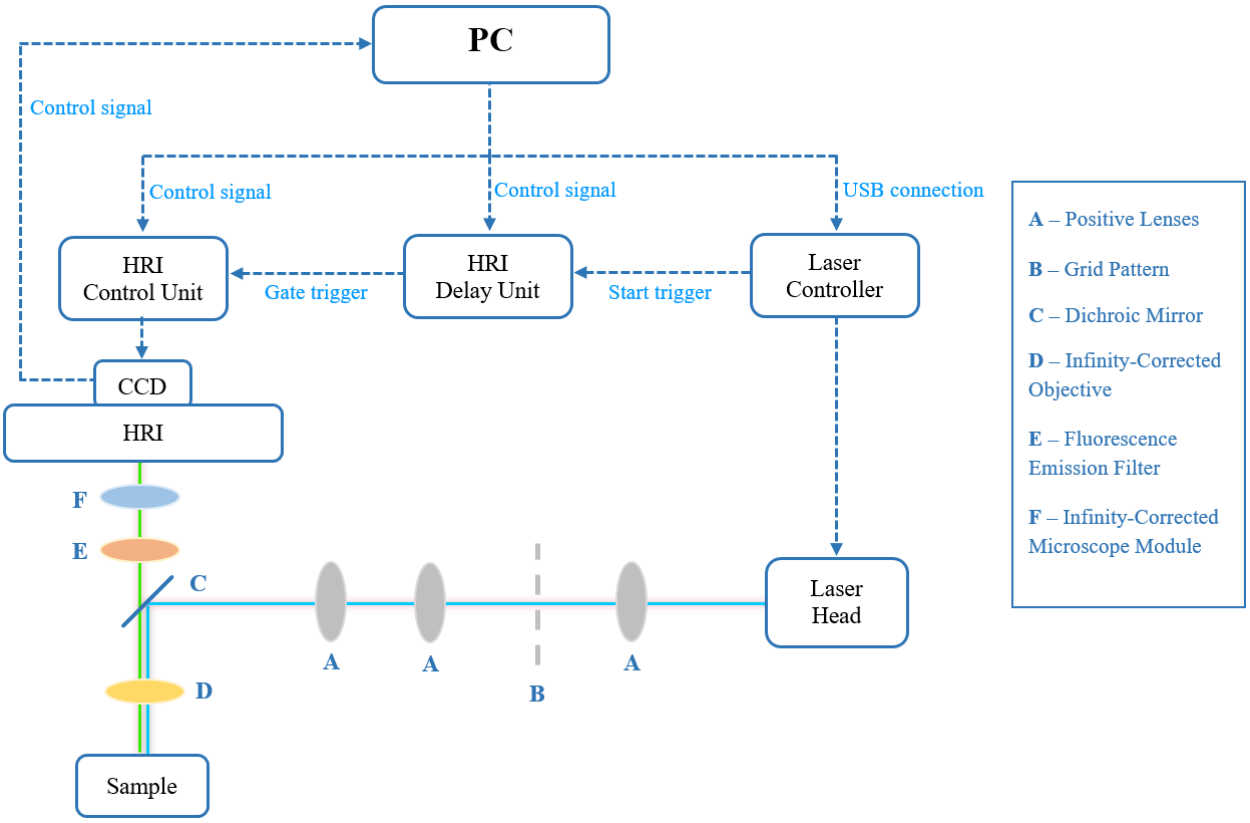

Figure 3.2 - Microscope Setup using the physical grid.

All the electronic components of the microscope are connected and can be controlled by a central unit, a PC which has installed the necessary software for each application.

3.2. Optical Components

3.2.1. Keplerian Telescope

The introduction of a Keplerian telescope onto the system was the first phase of this thesis. In chapter 4, we will study the reasons behind its implementation and the process of choosing the lenses. However, as it is a part of the microscope, a brief introduction will be presented.

The Keplerian telescope was invented by Johannes Kepler in the 16th century. This device is a combination of two convergent lenses that produces a magnification according to the chosen lenses. In our FLIM microscope it has the function of expanding the laser beam in order to fill the entire field of view of the detector.

The chosen convergent lenses are plano-convex in order to reduce spherical aberrations. The first lens, placed after the DMD, has a focal distance f=150mm and the second a focal distance of 100mm, providing a magnification of approximately 1.5x.

The telescope ensures that incoming parallel rays will leave as parallel rays, that is, if the object is in infinity, the image will also be in infinity.

Following the telescope, lays another positive lens with focal distance f = 125mm which will focus the rays onto the back focal plane of the objective.

The three lens are from the same manufacturer, Thorlabs.

Table 3.1 - Specifications of the three convergent lenses used in the microscope.

	LA1509-ML	**LA1433-ML**	**LA1509**
Glass Type	N-BK7	N-BK7	N-BK7
Type of lens	Plano-Convex	Plano-Convex	Plano-Convex
Optic Diameter (mm)	25.40	25.40	25.40
Focal Length (mm)	100	150	100

3.2.2. Dichroic Mirror

The dichroic mirror has a cutoff wavelength, being reflective to light with wavelengths lower than the cutoff limit and transmissive for higher wavelengths. As fluorescence light is emitted with a higher wavelength than the corresponding excitation light, a careful selection of the dichroic mirror allows to separate excitation and detection pathways.

In the microscope setup, the used dichroic mirror (DMLP 490, Thorlabs GmbH, Germany) has a cutoff wavelength of 490nm.

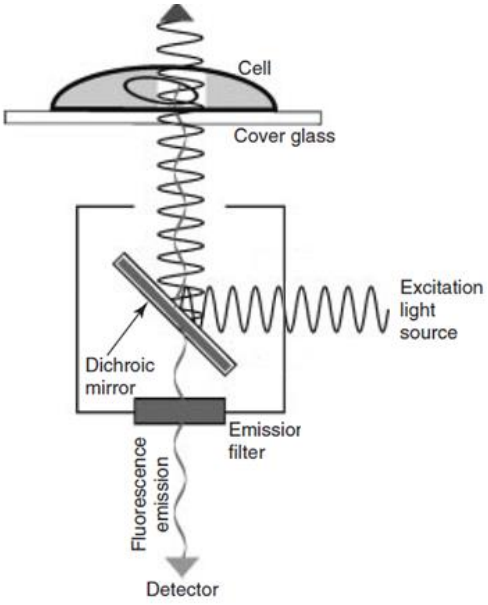

Figure 3.3 - Schematic of a Dichroic mirror. (Kubitscheck, 2013)

3.2.3. Objectives and tube lens

The objective is one of the most important and complex components of any light microscope as it is responsible for focusing the light onto the sample with minimal aberration and then collect and magnify the emitted signal. It is associated with the tube lens which will focus the image on the CCD camera.

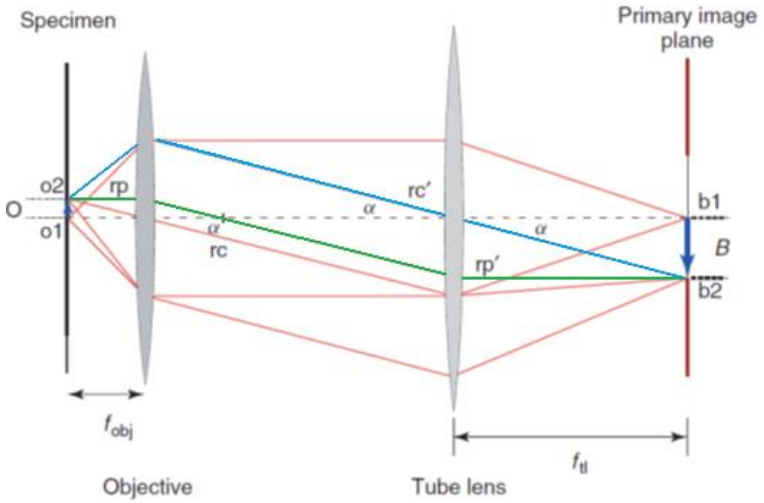

Figure 3.4 - Infinity-corrected imaging process. Infinity-corrected imaging process using light-sensitive array detector as image detector. (Kubitscheck, 2013)

In Figure 3.4, we can see the image formation process of an object with a height O, resulting in an image with height B. The angle α will be used to determine the system magnification in function of the focal distances of the objective, f_{obj}, and the tube lens, f_{tl}. The abbreviations rp and rc represent the parallel and central ray respectively. (Kubitscheck, 2013)

By a simple analysis of the image it is easy to notice that the magnification M of the system will be:

$$\boldsymbol{M = \frac{B}{O}} \tag{3.1}$$

Since the objective projects an image in infinity, any ray leaving the same position of the object will become parallel after crossing the objective. In the image, there are represented two rays in that situation, painted in green and blue. The green ray, rp, emitted parallel to the optical axis, is focused into the back-focus point of the objective lens. It forms an angle α with the axial plane of the lenses, so the objects height, O, can be written as a function of α and the focal distance of the objective. (Kubitscheck, 2013)

$$\boldsymbol{\tan(\alpha) = \frac{O}{f_{ob}}} \tag{3.2}$$

The second ray was selected for being a central ray to the tube lens. Since it is parallel to the previous ray, it forms the same angle with the axis and similarly the image height can be written.

$$\boldsymbol{\tan(\alpha) = \frac{B}{f_t}} \tag{3.3}$$

Using the three equations, the magnification can be simple written as:

$$\boldsymbol{M = \frac{f_t}{f_{ob}}} \tag{3.4}$$

This way, the magnification of this system could be written as a relation to the focal distances of the tube lens and the objective.

In the microscope, the tube lens is always the same, so the magnification of the system lays on the choice of objective.

Concerning the tube lens, using longer focal lengths produce smaller off-axis angle for diagonal light rays, reducing system artefacts. However, the tube length must be proportional to the focal

lens of the tube lens, making the optimal focal length value on the region of the 200mm. The objective has a minimum focal length value, so the magnifications of this combination usually ranges from 2 to 200. (Kubitscheck, 2013)

Another important characteristic of the objective is the numerical aperture. We have seen in chapter 2 that it is a function of the refractive index of the surrounding medium, n, and of the angular aperture of the objective, α and corresponds to the maximum angle at which the emitted light from the sample is still collected, as shown in Figure 3.5.

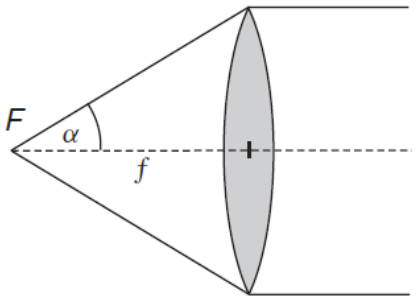

Figure 3.5 - Angular aperture of an objective. (Kubitscheck, 2013)

The results presented in the latter chapters of this thesis were acquired using an Achroplan objective from the manufacturer Zeiss, shown in Figure 3.6.

Figure 3.6 - Zeiss Achroplan objective.

The specifications of the objective are presented in Table 3.2.

Table 3.2 - Specifications of the objective Zeiss Achroplan N.

	Zeiss Achroplan N
Magnification	40x
Numerical Aperture	0.75
Working Distance (mm)	2.10
Cover Glass Thickness (mm)	0
Immersion Liquid	Water

3.3. Light source

The microscope source of light is a 63 ps, 40 MHz pulsed diode laser system composed by a laser head (PicoQuant LHP-O-C-440M, Berlin, Germany) with a central wavelength of 443 nm connected to a multichannel picosecond laser driver (PicoQuant PDL828). The laser head is shown in Figure 3.7.

Figure 3.7 - PicoQuant Laser Head

The main characteristics of the laser are present in Table 3.3.

Table 3.3 - Specifications of the diode laser

Wavelength	443 nm
Maximum Mean Laser Power	22.50 mW
Maximum Pulse Repetition Frequency	40 MHz
Minimum Pulse Width (FWHM)	63 ps
Maximum Pulse width (FWHM)	190 ps

Connected to the diode laser is a laser controller. This module, controlled by a software installed in the PC, is responsible for controlling the power of the laser beam and, more important, for providing the trigger to the HRI delay unit that starts the system.

3.4. Digital Micromirror Device

A Digital Micromirror Device (DMD) (DLP LightCrafter EVM, Texas Instruments Inc., Dallas, Texas, USA) is used for creating the pattern essential to structured illumination. This DMD is an array of microscopically small, square 684x608 switchable mirrors, regarded as pixels, each having two stable positions (+12º and -12º) which correspond to their ON and OFF states, respectively.

3.5. Acquisition System

The acquisition system is composed by four main components: A gated intensified CCD camera, a High Rate Intensifier, a delay generator module and a computer that controls the entire system.

3.5.1. Gated Intensified CCD Camera

In a camera based on a charged coupled device (CCD), an image is projected onto an array of semiconducting light-sensitive elements that generate an electric charge proportional to the intensity of the incident light. These light-sensitive elements are p-channel metal oxide semiconductor (pMOS) capacitors, usually called as pixel, as represented in Figure 3.8.

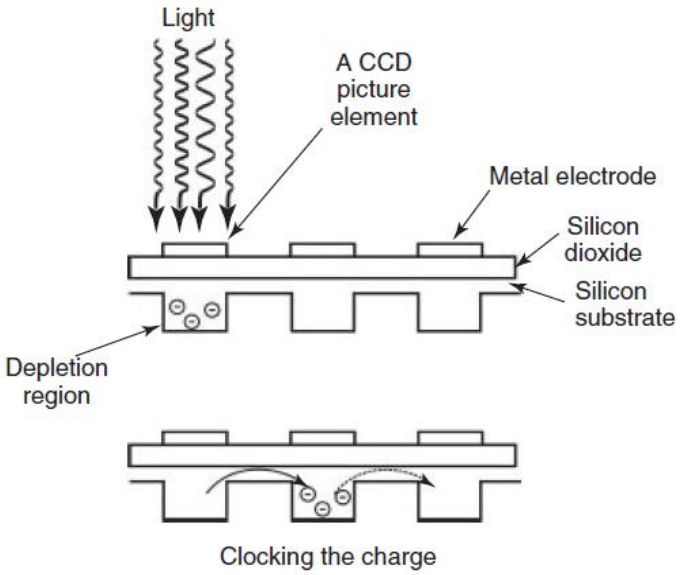

Figure 3.8 - Conversion of the photons into electric charges and their transfer in a CCD array (Kubitscheck, 2013)

When the pixels are exposed to light, each of them will accumulate an electric charge proportional to number of detected photons on the pixel area. After the exposure time, the accumulated charges are sequentially shifted, one line at a time, into an amplifier that will convert them into a corresponding voltage value until. Figure 3.9 represents this process.

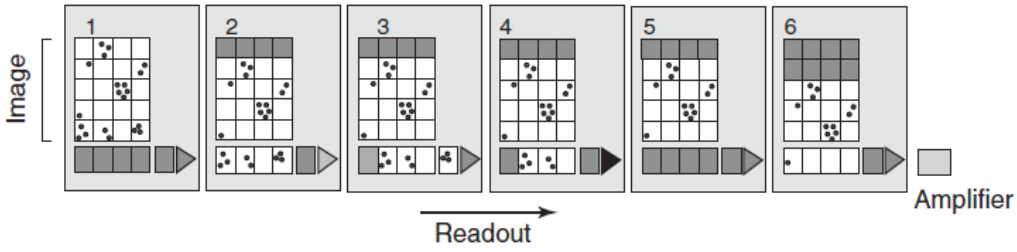

Figure 3.9 - Charge transfer in a CCD image sensor. (Kubitscheck, 2013)

Once this process is finished, the voltage values are converted into the levels of brightness, or simply intensity of light, on the display screen. Figure 3.10 shows the internal processes from the detection of the pattern until the resulting signal.

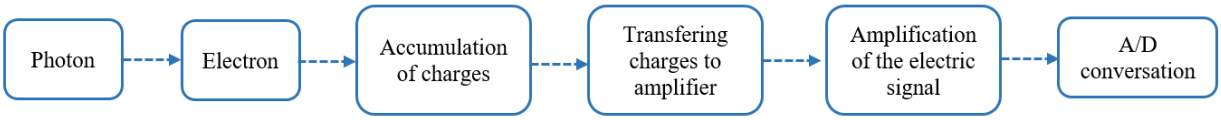

Figure 3.10 - A schematic representation of the steps occurring from the absorption of a photon in a CCD array to the display of brightness on a computer screen.

In fluorescence microscopy the signals are usually weak. If we also consider the need for high speed data recording, i.e., the use of ultra-short gates and it is easy to understand that a normal CCD camera would have difficulties separating the weak fluorescence signal from the readout noise. To cope with this problem, instead of a CCD camera, an intensified CCD (ICCD) camera is chosen. While a CCD camera can only produce one electron per incoming photon, an ICCD camera generates thousands of electrons per each photon. (Kubitscheck, 2013)

In the ICCD camera, a standard CCD light sensor is coupled to a light intensifier device. The intensifier consists of a photocathode, a micro-channel plate (MCP) and a phosphor screen as shown in Figure 3.11. When a photon hits the photocathode, it may generate an electron through photoelectric effect. Due to a strong electric field, created by an electric control voltage between the photocathode and the MCP, the electron is accelerated towards the MCP layer. The electron will hit the metal-coated inner walls of the MCP channels, generating further secondary electrons that will reach the phosphor. There, each electron will cause the emission of a photon that will be collected by the CCD camera. (Kubitscheck, 2013)

The voltage applied between the photocathode and the MCP generates the electric field necessary to accelerate the electrons towards the phosphor screen. However, this voltage can be reversed, changing the direction of the electric field. When this happens, the electrons will no longer be accelerated onto the phosphor layers but instead return to the photocathode. This process is called gating and defines the minimum exposure time. This process reduces significantly the signal to noise ratio in comparison with a regular CCD camera. Therefore, image acquisition implies a large number of gating procedures to obtain an adequate signal-to-noise ratio

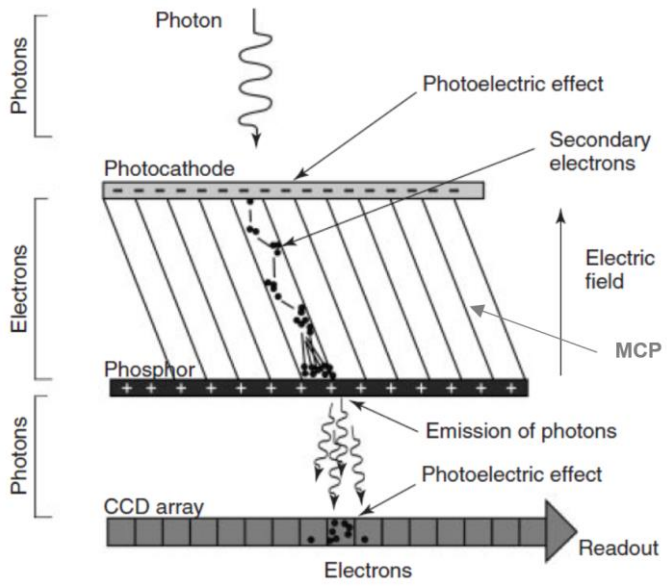

Figure 3.11 - Signal amplification in an intensified CCD sensor. (Kubitscheck, 2013)

In the system, the CCD chosen is an imager compact from LaVision with an array of 640x480 micro-mirrors of size 9.9x9.9 μm2. The readout of the pixels ranges from 6.8 to 24.8ms. The spectral range covers from 280 to 1000nm, which includes all wavelengths expected from fluorescence emission.

3.5.2. High Rate Intensifier.

The High Rate Intensifier (HRI) has two main elements. The image intensifier is directly connected to the CCD camera and acts, as we have seen, as an image amplifier. This module, the PicoStar HR produced by LaVision, consists of a S25 photocathode, a single microchannel plate and a P43 phosphor screen is shown in Figure 3.12.

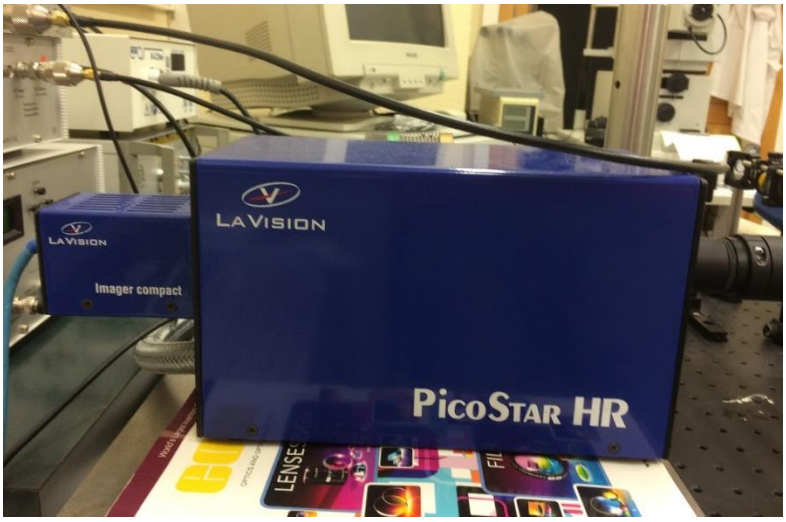

Figure 3.12 - High Rate Intensifier

An HRI controller module, shown in Figure 3.13, is connected to the computer via USB connection and is responsible for controlling the CCD camera gating and the intensifier gain.

Figure 3.13 - HRI controller Module

The HRI gain is set by controlling the voltage of the MCP that defines the electrical field within the intensifier. The relation between the voltage of the MCP and the gain is expressed in the following table.

Table 3.4 - Resulting gain as a function of the difference of potential of the MCP.

UMCP [V]	Gain (cnts/el]
260	0.01
300	0.02
350	0.06
400	0.17
450	0.43
500	1.05
550	2.41
600	5.20
650	11.10
700	21.60
750	45.00

Finally, the camera gating is defined by a Transistor-Transistor Logic (TTL) trigger generated by the module after receiving the trigger from the HRI delay unit.

3.5.3. HRI Trigger Delay Module

This module is connected to the laser controller, the PC and the HRI controller module and is crucial for the system being able to perform lifetime measurements. It allows to sample fluorescence emission at different locations of the fluorescence decay curve
While the laser is on, it accepts triggers from the laser controller. Its function is to redirect those triggers to the HRI controller module with a specific delay. This unit is controlled by a software installed in the PC through a RS232 interface which will be responsible for defining the delay. This module is shown in Figure 3.14.

Figure 3.14 - HRI trigger delay module

The resolution of the delay module used in the system is 1ps. The delay range is from 0 to 50ns.

4. METHODS

4.1. Simulation of Kepler telescope

When I started my project, the microscope could not fill the entire field of view of the CCD camera. This meant the microscope was not working to its full potential. To solve this problem, it was necessary to design a system of lenses that would magnify the laser beam.

There are many factors that needed to be taken into consideration when designing an optical system. Having the correct focal distance is not enough. In our design, limiting aberrations was a major concern. To cope with this problem, an optical design program, Zemax, was used for simulating the design and analysing the performance of the system.

The software Zemax OpticStudio 15 is a Computer Aided Design (CAD) tool capable of simulating an optical path of a lens system and provide information regarding the performance of the design.

4.1.1. Requirements of the system

Before starting the process of lens selection, it was necessary to consider the conditions and restrictions presented by the microscope system.

In terms of limitations, the most significant one was the available space. The DMD handles the light beam in a similar way to a diffraction grating. So, if we were to enlarge the beam before it strikes the DMD, it would result in loss of intensity at the first order and increase at higher orders. Therefore, the Keplerian telescope had to be placed after the DMD, reducing the available space to a maximum of 40cm.

In terms of magnification, the system required the beam to be enlarged a factor of 1.5-2x. Also, it is worth mentioning that the illumination is monochromatic, meaning that only monochromatic aberrations had to be taken into consideration.

4.1.2. Optic Aberrations

One of the set stones of modern optics is based on the paraxial ray theory, which is based on the assumption that sin(φ) = φ, i.e., that the optical system is only used inside a small region around the optic axis. (Hecht, 2012)

In real systems, though, it is necessary to assume that all the lens aperture may be used, making the paraxial theory no longer valid as the marginal rays are considered. (Hecht, 2012)

By considering the marginal rays, it becomes necessary to expand the initial first order theory into higher orders, per

$$\boldsymbol{sin(\varphi) = \varphi - \frac{\varphi^3}{3!} + \frac{\varphi^5}{5!} - \frac{\varphi^7}{7!} + \cdots} \quad (4.1)$$

When we consider the cubic term, we get the five basic optical aberrations. These aberrations were originally studied by Ludwig von Seidel, during the 1850's, and are often referred to as Seidel aberrations. The later terms give origin to higher order aberrations and are often neglected. (Hecht, 2012)

The five primary aberrations are represented in Figure 4.1.

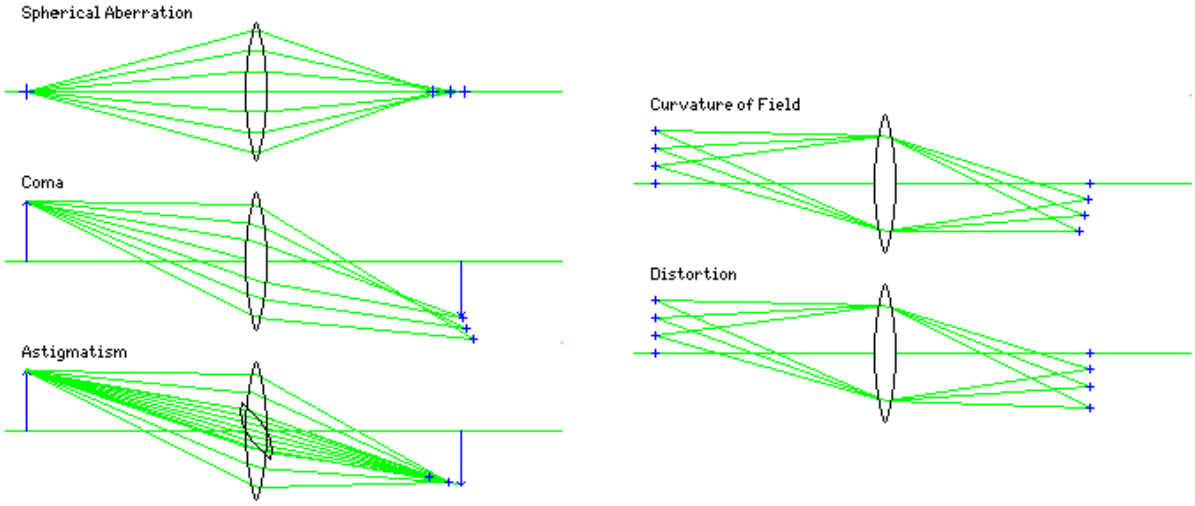

Figure 4.1 - Seidel aberrations. (Quadibloc)

4.1.3. Keplerian telescope

After knowing the system requirements, it was necessary to design a solution to fill the field of view of the objective. The first option to be considered was creating a small Galilean telescope. The Galilean telescope, as represented in Figure 4.1, uses a convergent lens closer to the object followed by a divergent lens to focus the beam. Although the distance between lenses in the representation of the Galilean telescope of Figure 4.1 is not correctly scaled for a real system, it gives a good notion of the telescope function.

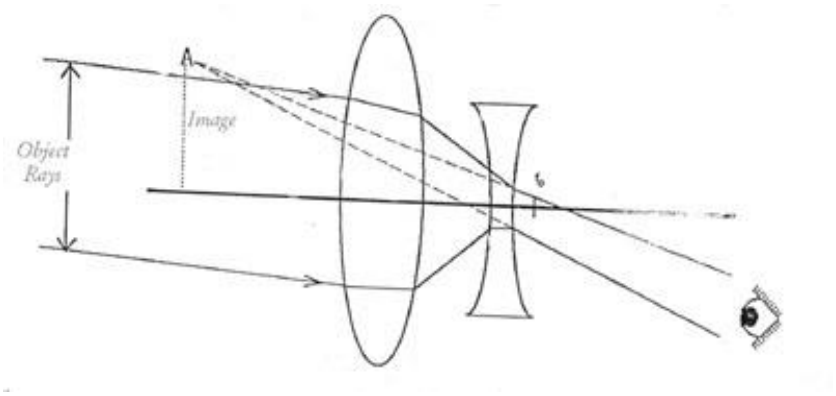

Figure 4.2 - Non-scaled Galilean telescope. (Richards, 1997)

After testing the Galilean telescope with several combinations of lenses, we concluded that the aberrations it would create onto the system where not acceptable. Therefore, a Keplerian telescope was tested to see if it met the requirements of the system. This telescope uses two convex lenses. The first is responsible for focusing the object into an intermediate point between the two lenses, while the second one focus the image onto the target, or as represented in 4.2, the eyepiece.

The main disadvantage of the Keplerian telescope, when comparing with the Galilean's, is the inverted image. However, it the context of the microscope, that does not pose a problem. Figure 4.2 is a representation of a Keplerian telescope.

If the two lenses are correctly spaced, the magnification is given by the ratio between the focal distance of the objective and the eyepiece, as expressed in equation 4.2.

$$\boldsymbol{M = \frac{f_{ob}}{f_{eye}}} \tag{4.2}$$

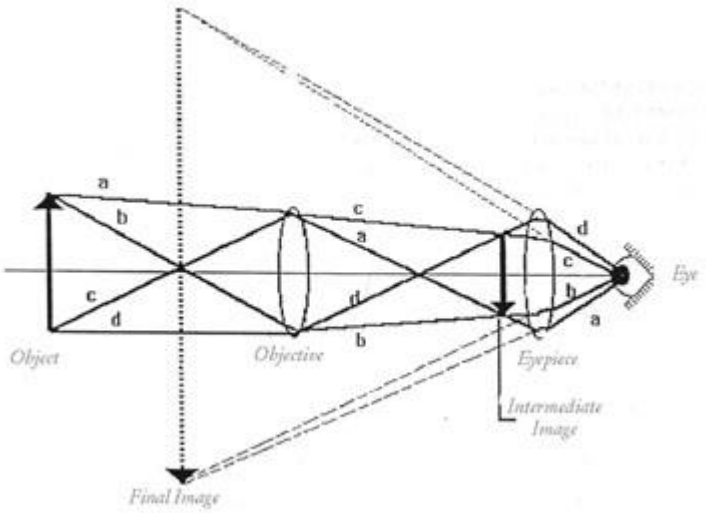

Figure 4.3 - Non-scaled Keplerian Telescope. (Richards, 1997)

As the Keplerian telescope tested met the requirements, two convergent lenses with focal distances of 150 mm and 100 mm were introduced in the system, providing a magnification of 1,5x. Both lenses were plano-convex to reduce the effect of spherical aberration.

4.2. Acquisition Software

The acquisition software is a crucial part of the microscope system as it must configure and manage all electronic components of the microscope while presenting the image acquired by the CCD camera to the user and, when required, store the acquired data of the image.

4.2.1. DaVis Software

In the description of the components of the system it was mentioned that all the electronic components of the acquisition system shared the same manufacturer to ease their integration. The software used for this purpose was developed by LaVision and is called DaVis.

The DaVis software controls the exposure time of the CCD, the voltage between the photocathode and the MCP of the intensifier, i.e., the gain, the delay imposed by the HRI delay unit as well as the acquisition configuration.

4.2.2. Acquisition Configuration

For this work, the DaVis software was used in two configurations: the General Image Recording Interface and the General Scan Recording Interface. The first mode is used for the acquisition of single images. Here, the user must define the operating parameters. It is necessary to set the exposure time of the sample, the voltage of the image intensifier, the resolution of the image and the delay of the system.

After defining the operating parameters, the software is continuously acquiring images, allowing the user to adjust the position of the sample until finding a suitable image. Then the user stops the acquisition and may save the acquired image.

The second mode is used for fluorescence lifetime measurements. The user defines the configuration of the system and the system acquires the specified number of images with incrementing delays.

Figure 4.4 shows the interface of the LaVision Davis software, where it is possible to control the exposure time of the system, the MCP voltage, and thus the gain, and the delay of the system.

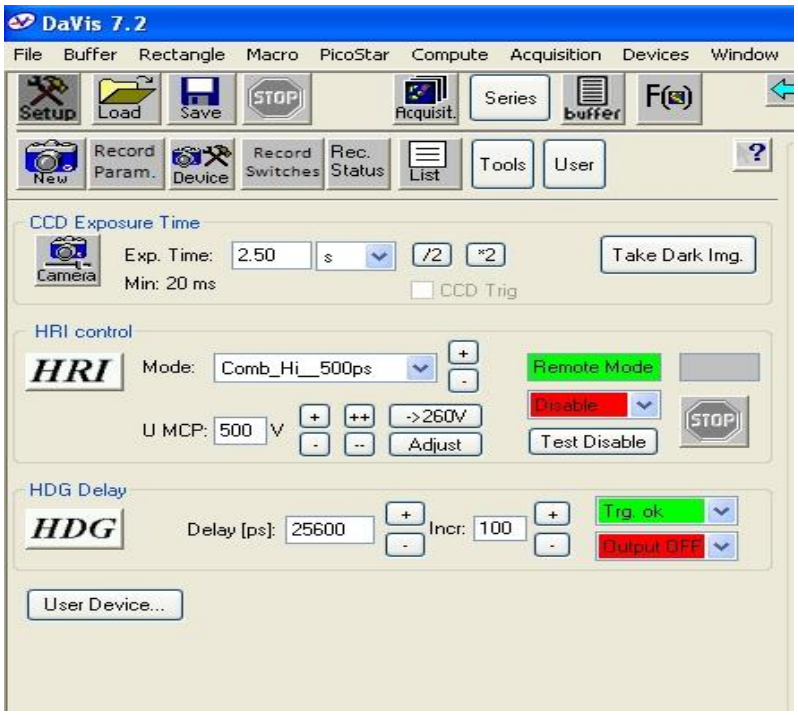

Figure 4.4 - Configuration dialog from DaVis Software.

4.3. Data Processing

After acquiring the images, it is necessary to process them to obtain a sectioned imaged with adequate quality in terms of optical sectioning and contrast.

The structured illumination microscopy and HiLo microscopy methods are applied and combined with image processing techniques using the high-performance coding software Matlab.

The code was developed to be as automatized as possible. In fact, for both techniques, the user only needs to input the images and run the code to obtain the final image.

In this chapter, we will present the applied image processing. The full version of the codes is presented in Annex A and B.

4.3.1. Structured Illumination Microscopy

In this section, we will present the most relevant operations concerning the implementation of the Structured Illumination Microscopy technique.

In Figure 4.5 we show a flow diagram concerning the software routine that implements the Structured Illumination Microscopy technique.

The first step consists on reading the images and converting them into a more appropriate format. The three acquired images (640x480 pixels) are stored in the '.IMX' format. To upload the images, we used a function developed specifically for that purpose by LaVision called readimx. Then, the image data is converted into an array of 480x640 double-precision values.

The following step consists on the application of a normalization by the average value on the three sectioned images. This ensures similar conditions of illumination for the three images The software calculates the average value on a region centred on a given pixel, for each of the three recorded images. Then the pixel value is normalised to the higher average value from the three images. This process is then repeated for all image pixels.

The only setback with this technique is that the margins of the image will not be altered. For example, if we use a 10x10 mask, the first and last 5 columns and lines will not be modified. Although the margins are not of extreme importance, since mostly correspond to out-of-focus background, this is a factor to consider when selecting the size of the masks. On the other hand, the size of the mask cannot be too small since this would make the normalization more susceptible to a peak of energy in any of the images.

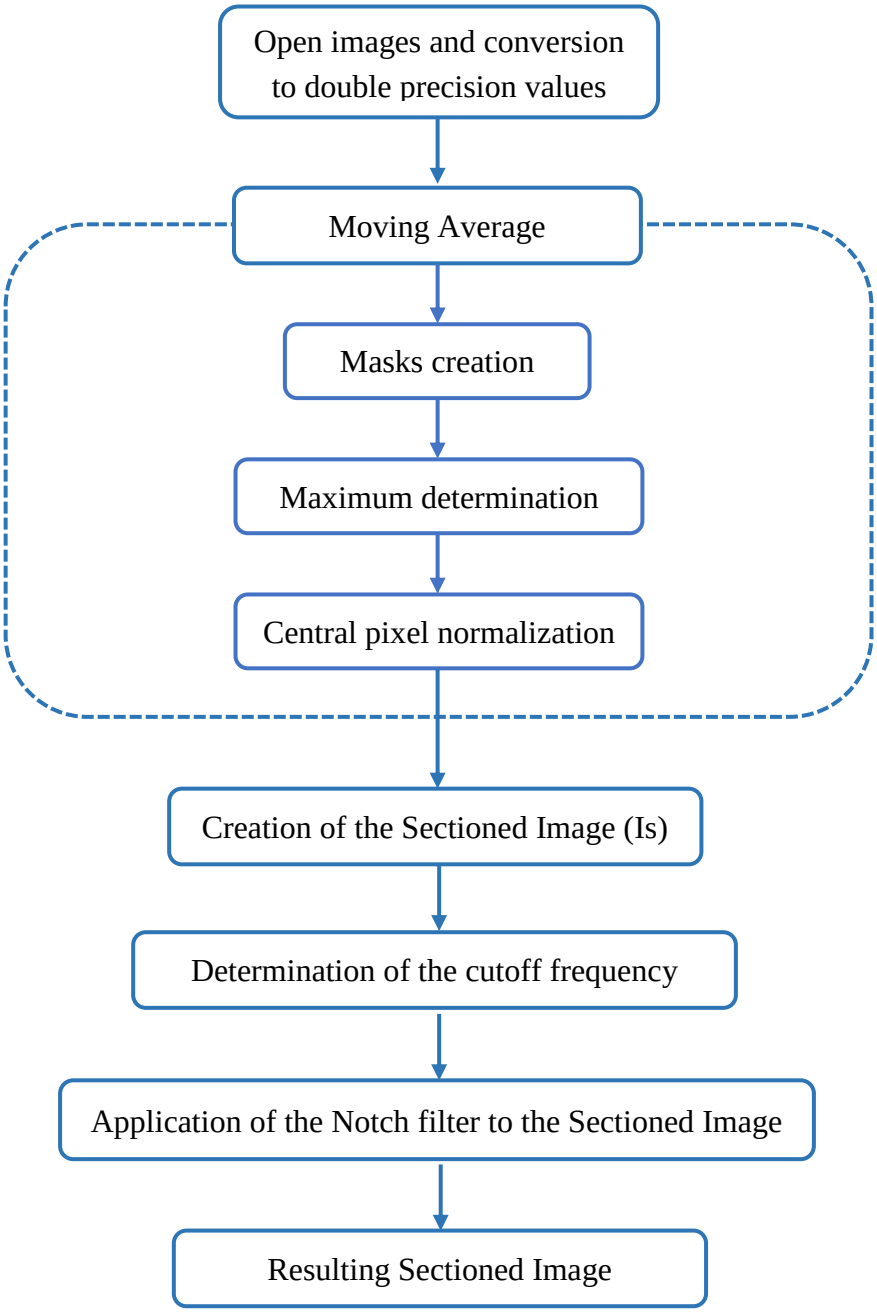

Figure 4.5 - Flow diagram of the SIM processing

To implement this method on Matlab, we created a cycle containing three steps after defining an adequate size for the masks. Firstly, it is necessary to create the correct mask at each iteration, i.e., define a matrix containing the values in the vicinity of the pixel being adjusted. Then, the average value of each mask is analysed and the average is stored for later use. The final step is to normalize the pixel of each image (the central pixel of the mask).

Following the normalization of the three structured illumination images, we get the sectioned image by applying equation 2.10. A notch filter will be applied to eliminate any residual pattern that may still be present on the sectioned image. However, it is necessary to determine first the fundamental frequency of the pattern.

Theoretically, the pattern frequency should be detectable on the Fourier spectrum of any image where the pattern is present. In practice, this process is not easy, mainly because only a small portion of the image has the pattern projected on it, making the peaks corresponding to the pattern harder to find due. A process that was considered was to define manually an area where the pattern is present and only transform that area to the Fourier domain. However, this method was discarded since our goal was also to make the process as autonomous as possible.

The chosen process consisted on the creation of a demodulation function, by subtracting one of the patterned images from the widefield image, per:

$$\boldsymbol{D = |I_c - I_1|} \tag{4.2}$$

where I_c represents the widefield image and I_1 can be either of the original images.

Figures 4.6 and 4.7 show the image spectrum of the centred Fourier transform and the plot of the columns average respectively, from the demodulation function obtained from one of the used samples.

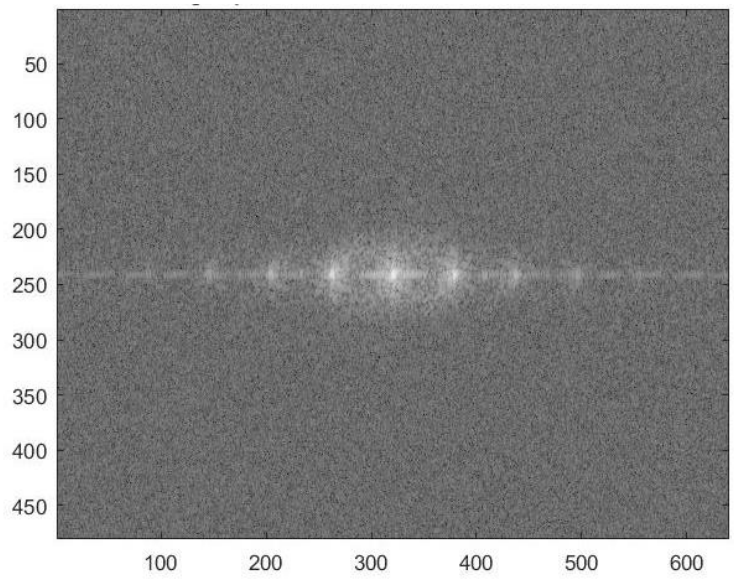

Figure 4.6 - Image spectrum of the demodulation function.

From Figure 4.6 we can see clearly the peaks resulting from the pattern and its harmonics.

On the software program, the demodulation function is declared according to equation 4.2, where the widefield image is obtained by the average of the three structured images, as referred in equation 2.11. The fundamental frequency is obtained by determining the position of the first peak on the Fourier transform of the demodulation image column average. As shown in Figure 4.7, this is a one-dimensional array of values.

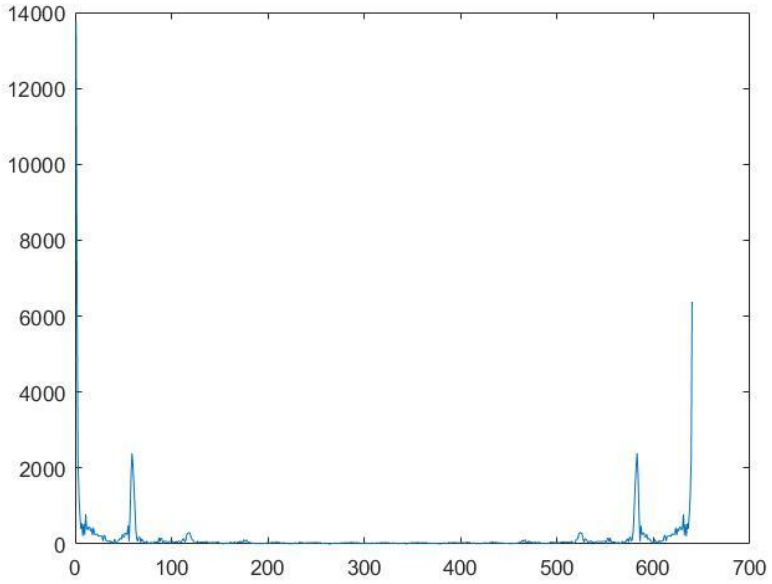

Figure 4.7 - Column average of the demodulation image.

Finally, three Gaussian Notch filters are applied to the sectioned image at the wavelengths of the fundamental frequency and the first two harmonics.

4.3.2. HiLo Microscopy

Similarly to the previous chapter, in Figure 4.8 we show a simple flow diagram of the HiLo program. This method requires two images: a uniform and a structured illuminated image.

The first step in HiLo processing is exactly equivalent to the first step on SIM processing and concerns reading the images.

The demodulation image can be created by applying equation 2.13. However, as it was mentioned in chapter two, the use of a grid reduces the amount of light projected onto the sample. In the theoretical approach, this light loss was compensated by introducing a factor of two in equation 2.13. At this stage, we calculate the ratio as a function of the mean intensities of the uniform and structured images, Iu and In per:

$$\boldsymbol{Ratio} = \frac{\boldsymbol{Mean}(\boldsymbol{I_u})}{\boldsymbol{Mean}(\boldsymbol{I_n})} \quad (4.3)$$

The next step is to determine the fundamental frequency of the pattern. This step was already described and explained on the SIM code.

Then we apply a Gaussian high pass filter to the demodulation image. This high pass filter simply ensures that the demodulation function D is centred around zero, as we have seen in chapter 2.

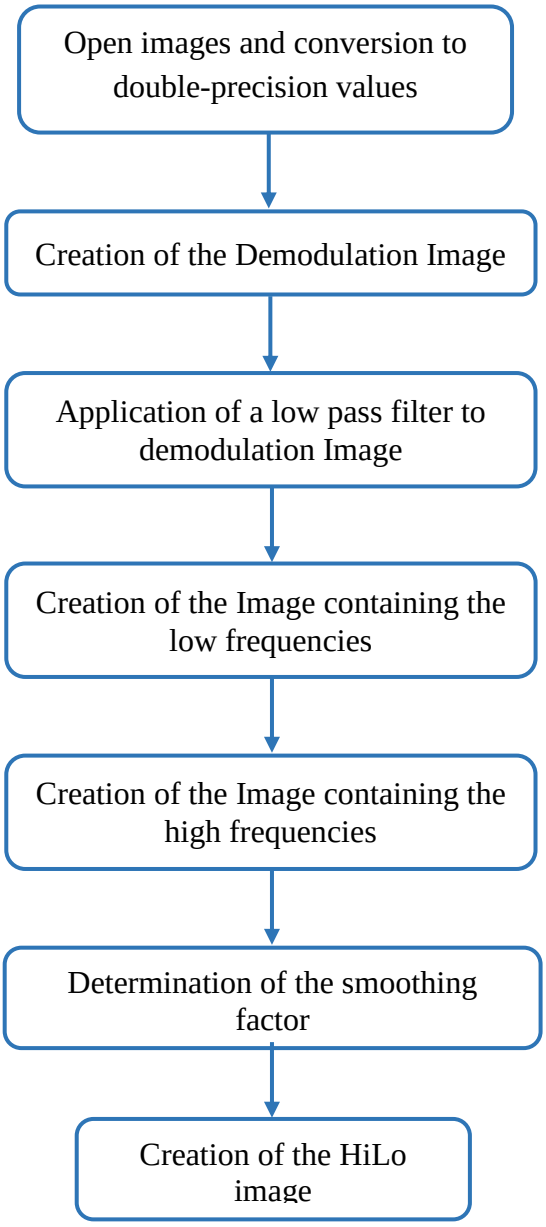

Figure 4.8 - Flow diagram of the HiLo processing

In order to obtain the low frequency image, I_{Lo}, a low pass Gaussian filter with frequency slightly smaller than the cutoff frequency is applied to the demodulation image.

The high frequency information is obtained from the uniform image by applying a complementary high pass filter, that is, with the same frequency as the low pass filter used on the demodulation image.

The final step combines the information contained in the two images, the Hi and Lo components. Firstly though, it is necessary to calculate the scaling factor, n, responsible for ensuring a smooth transition across the cutoff frequency. For that, we apply a band pass filter, with a narrow passband centred in the cutoff frequency, to both the Hi and Lo frequency images. The scaling factor is obtained by dividing the total intensities of their Fourier transforms.

The final step is the calculation of the HiLo image, which is achieved by applying equation 2.18.

4.4. Resolution of the microscope

In chapter 2, we have seen the theoretical approaches to determine the lateral and axial resolution of the microscope. As structured illumination aims to achieve optical sectioning, we will discuss in this section the approach to obtain the theoretical axial resolution from equations 2.19 to 2.21 and the methods to determine the actual sectioning power of the microscope.

In chapter 5 the resulting axial resolution will be presented and analysed for the two set-ups used, i.e., when the pattern is generated by the DMD and by the physical grid.

4.4.1. Theoretical Resolution

Equation 2.19 represents how the image intensity decays with defocus. The wavelength, λ, magnification and numerical aperture of the objective, M and NA respectively, the focal distance of the tube lens, ft, and the refractive index of the used optical coupling gel, n, are fixed values defined by their manufacturers.

The focal lens of the lenses imaging the grating onto the back of the objective had to be calculated by considering the several lenses as a single lens and measuring the distance between them. For example, for a system of two lenses the simplified focal distance is given by:

$$\frac{\mathbf{1}}{\boldsymbol{f}} = \frac{\mathbf{1}}{\boldsymbol{f_1}} + \frac{\mathbf{1}}{\boldsymbol{f_2}} + \frac{\boldsymbol{d}}{\boldsymbol{f_1 f_2}} \tag{4.4}$$

where f_1 and f_2 are the focal distances of the two lenses and d is the distance between them.

It also necessary to know the frequency of the grid pattern. In case it is a physical grid the value is defined by construction. However, when the DMD is used, the frequency needs to be determined considering the size of the micromirrors and the spatial frequency of the pattern.

Finally, the theoretical axial resolution corresponds to the Full Width Half Maximum (FWHM) of the plotted values of the axial intensity profile, I_p.

4.4.2. Measuring axial resolution

To measure the resolving power of the microscope, a target was painted with a fluorescent dye and placed on top of a micrometre board capable of moving the target along the axial direction with a precision of 0,5 μm.

Starting at a position where the pattern is not visible, the target is elevated and an image is acquired at each axial step, passing through the position where the pattern is on focus until it is no longer visible.

Earlier it was said the optical sectioning strength is defined as the axial distance between two points at which the intensity of the sectioned image has half the value of that when the grating is in focus. The position where the grid is on focus corresponds to the normalized spatial frequency, that is, the first order of the pattern.

Firstly, the spatial frequency of the grid is determined on the image where the pattern is most visible and then, the intensity at that frequency from the column average of each image is recorded in an array of values.

The measured values correspond to the intensity image with defocus, I_p, and the axial resolution is the FWHM of this intensity profile.

4.5. Lifetime Mapping

The main goal of fluorescence lifetime microscopy is to create a lifetime map of a sample, i.e., determine the fluorescence lifetime at any point of the sample.

The process to create a fluorescence lifetime map can be divided in 3 phases: image acquisition method, image processing and display of the results.

As mentioned early, to create a fluorescence lifetime map it is necessary to acquire a set of images. This is done by defining the initial and ending delay, as well as its increment. Let’s say

the starting delay is at 2000ps and the ending delay is 20000ps with an increment of 200ps. This would result in 91 images. If the sectioning method is SIM, which requires three images for each delay, this results on a total of 273 images that need to be analysed. For HiLo the total number of images would be 182.

The images need to be processed independently for each delay. This is the main reason why the optical sectioning processing routines were designed to operate as autonomous as possible instead of leaving to the user the task of finding the cutoff frequencies.

After the images are processed using the techniques described in this chapter, they must be stored externally, as we chose to use the established reference software FLIMfit to perform the fitting of the decay curves and determine the fluorescence lifetimes.

FLIMfit is a tool specifically designed to analyse and visualize time-resolved data from FLIM experiments. This program incorporates image segmentation using an extremely efficient algorithm to fit the provided data into the corresponding exponential decay. (FLIMfit)

Figure 4.9 shows the intensities of an image pixel along the acquired images as seen in FLIMfit. The program will then perform a mono- or a multi-exponential fitting to determine the fluorescence lifetime(s) at each pixel. In multi-exponential fittings, it is also necessary to determine the fractional contributions of each fluorescence lifetime.

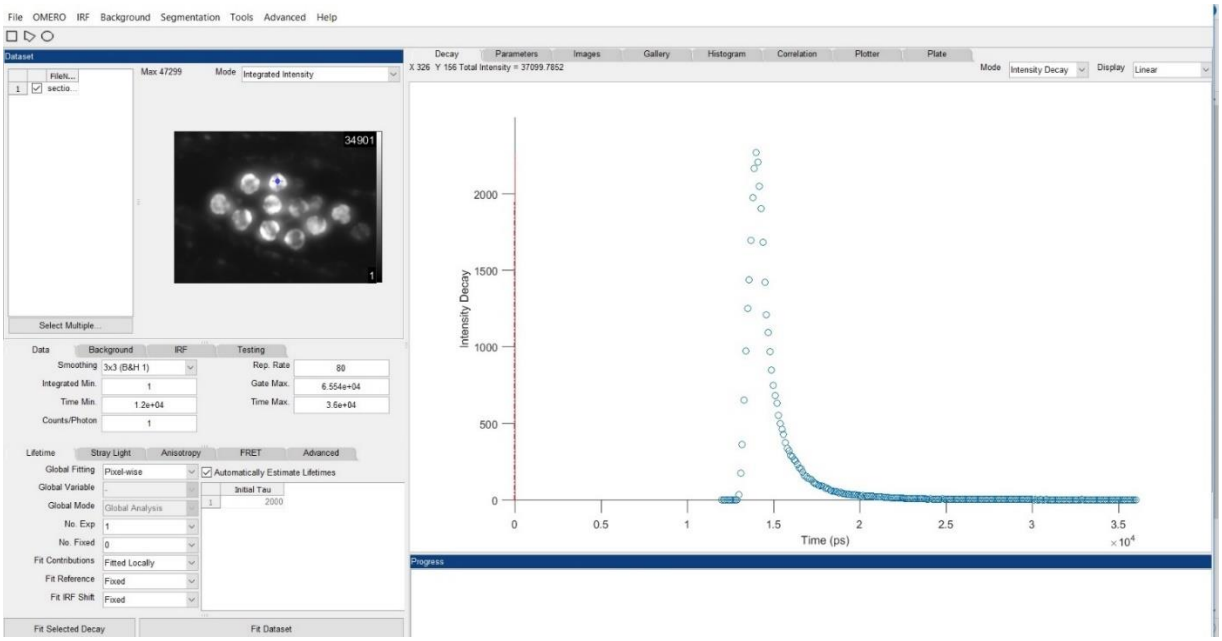

Figure 4.9 - Image analysis window of FLIMfit software

5. PERFORMANCE RESULTS AND ANALYSIS

This work would not be complete without presenting the results of the methods described on the previous chapter.

Firstly, we will see the results of the optical simulations concerning the Kepler telescope introduced in the system.

To test the performance of the whole set-up, i.e., the microscope and the post-acquisition software, samples of cotton fibres embedded in fluorescent dyes and pollen grains were processed using both sectioning methods.

After realizing tests to determine the effective optical sectioning power of the microscope, the presented methods were applied to produce fluorescence lifetime maps from a sample of pollen grains.

5.1. Optical Simulation

The simulation of the Keplerian telescope developed for the microscope is presented here, with more focus on the functions used on Zemax OpticStudio to evaluate the aberrations.

5.1.1. Keplerian Telescope Design

Figure 5.1 shows the simulations on Zemax of the optic path for an object located in infinity. The first two lenses, from left to right, are the ones being introduced into the microscope, while the third is a convergent lens already being used prior to the objective.

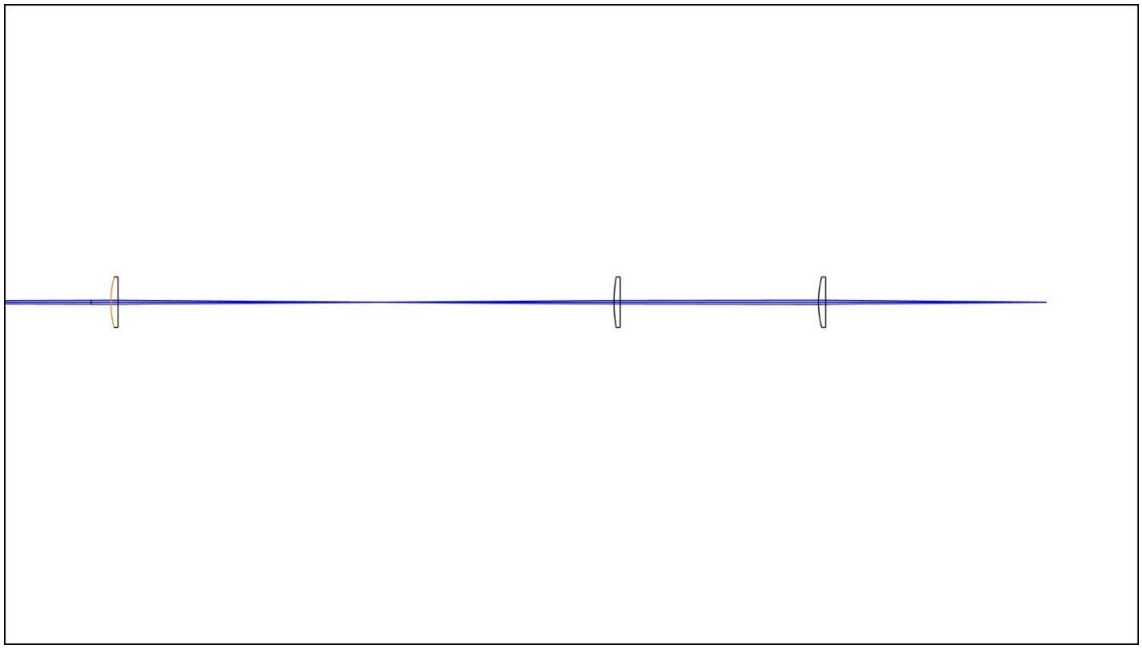

Figure 5.1 - Zemax OpticStudio simulation of three convergent lenses

5.1.2. Tests Performed

The first test is based on the Seidel diagram. The Seidel Diagram is a representation of the five primary aberration coefficients in the form of a histogram. It shows the relative weight of the various aberrations at each surface of the system and the sum of the individual aberrations. This is particularly useful in identifying the lenses that are causing aberrations and which aberration is more significant.

Figure 5.2 is the Seidel diagram of the two lenses being considered. The diagram divided each lens into the two surfaces. We can see that most of the aberrations are caused by the convex surfaces of the lenses (surfaces 3 and 5) which corroborates the initial assumption behind the choice of plano-convex lenses.

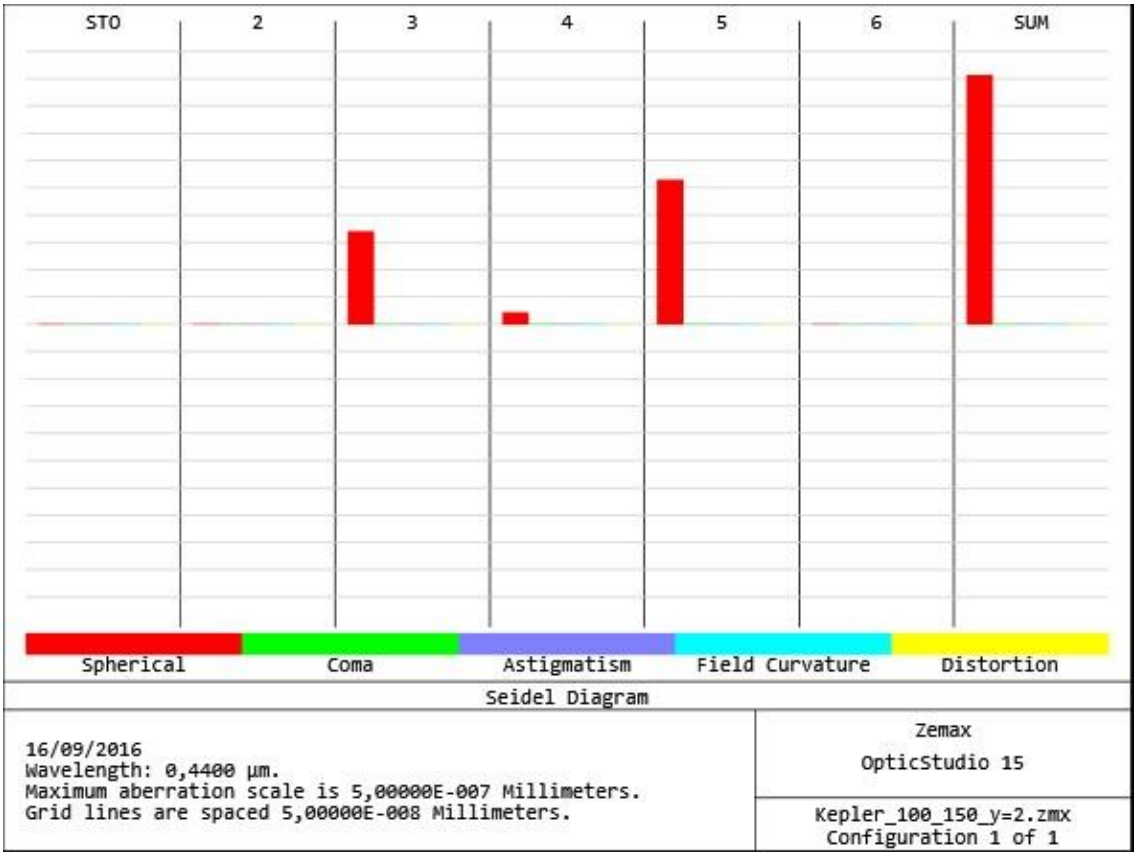

Figure 5.2 - Seidel Diagram of the Keplerian telescope.

Also from the Seidel diagram, we can see that spherical aberration is the only significant aberration. However, the histogram representation does not show the quantitative deviation along the optical axis caused by the lenses.

Spherical aberration is the result of a difference of focal distances between the central and paraxial rays, leading to different focal points in the optical axis. The spherical aberration of the Keplerian telescope is represented in Figure 5.3.

Using a pupil radius of 0,5 millimetres, the total spherical aberration due to the lenses is approximately 14µm, which we can see from observing Figure 5.4. This aberration may cause a decrease in the contrast of the projected pattern. However, this decrease will not be significant.

To conclude the analysis of the Keplerian telescope, Figure 5.4 shows the expected effect of projecting the image on the left through the lens system.

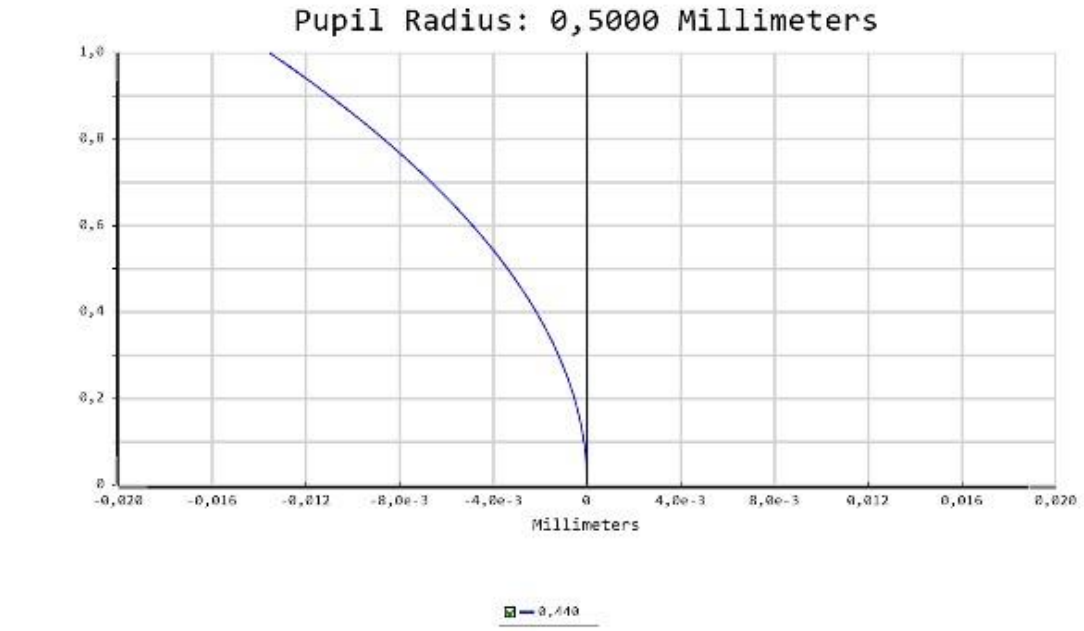

Figure 5.3 - Longitudinal deviation introduced by the Keplerian telescope.

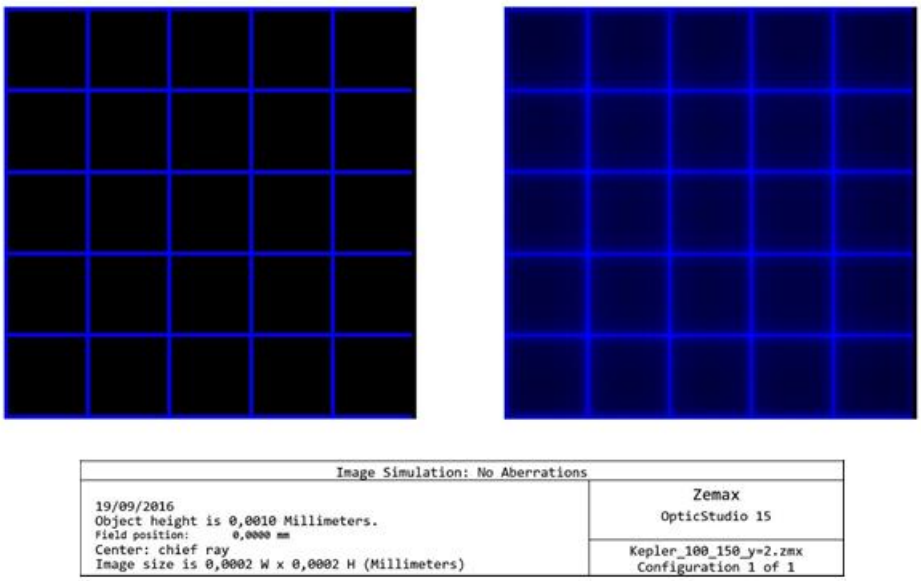

Figure 5.4 - Object (left) and Image (right) using the Keplerian telescope

This test showed the image formed by the two lenses considering only geometric aberrations. We can observe in Figure 5.4 that the result is a slightly blurred image when compared to the original. However, this effect when two lenses are tested is inevitable and, in this situation, it does not significantly degrade the quality of the image.

Overall, from the analysis presented above, it was considered that the aberrations caused by the introduction of the two lenses were acceptable and did not degraded the performance of the microscope. In fact, the implementation of the Keplerian telescope was relatively easy and fulfilled the goal of filling the field of view of the detector. The Kepler telescope did not cause any noticeable degradation of the images.

5.2. Imaging Tests Results

On this section, two samples were used to test and compare each technique's ability to eliminate the pattern and reconstruct a sectioned image.

In the SIM processing, the sectioned image can be called at any phase, allowing to observe the effect of each technique. This is not possible for HiLo microscopy, where we only have access to the final result because we do not receive any useful information from observing separately the high and low frequencies content.

In the introduction, it was mentioned that the evaluation of the results at this phase was mostly quantitative. Therefore, to analyse the performance of the SIM and Hilo processing there will be two parameters taken into consideration: the ability to reduce, and if so, eliminate the pattern and the out-of-focus information.

5.2.1. Structured Illumination Microscopy

In this chapter, for each method, we will see one of the initial images and the sectioned image at three distinct phases of their processing. Firstly, it will be presented the image without any processing. Then we will see the impact of the moving average mean normalization and finally the result after applying the notch filter for the sigma value that produced the best results.

5.2.1.1. Pollen Grains

In this section, we present the images resulting from the SIM processing, for pollen grain samples. The images are presented in greyscale to ease the analysis of the performance of the algorithm.

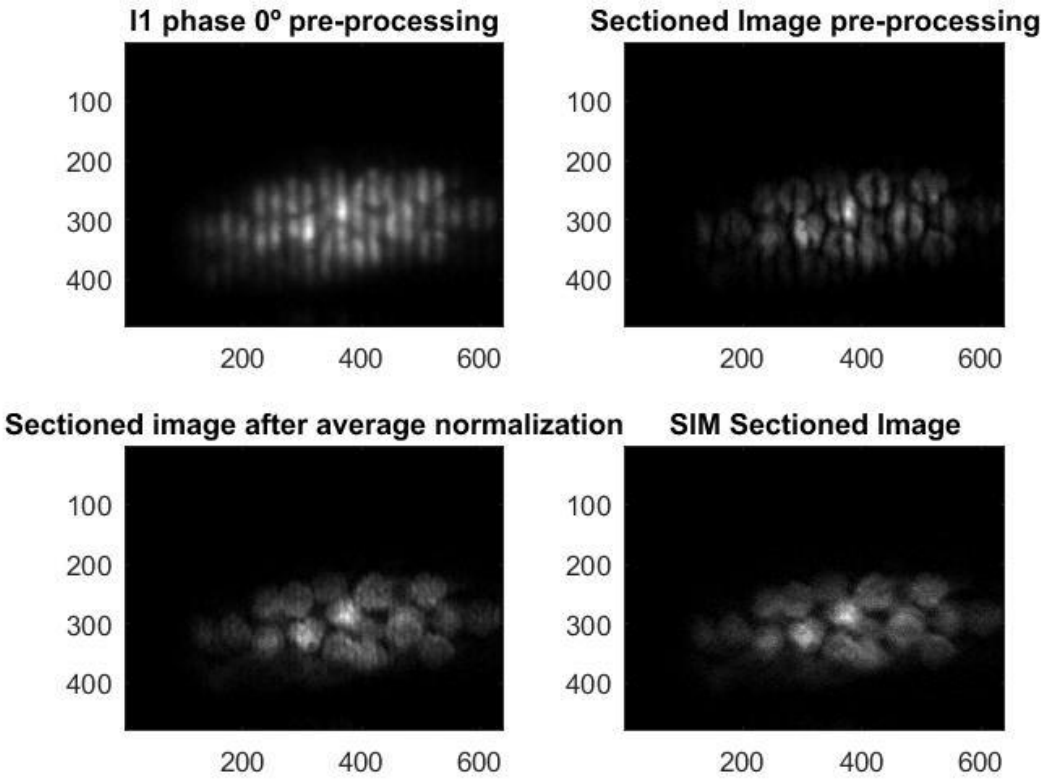

Figure 5.5 - The two images on top are the structured (left) and sectioned (right) images of a sample of pollen grains, without any processing. The images on the bottom side are the sectioned image following the average normalization (left) and the final sectioned image (right).

5.2.1.2. Cotton Fibres

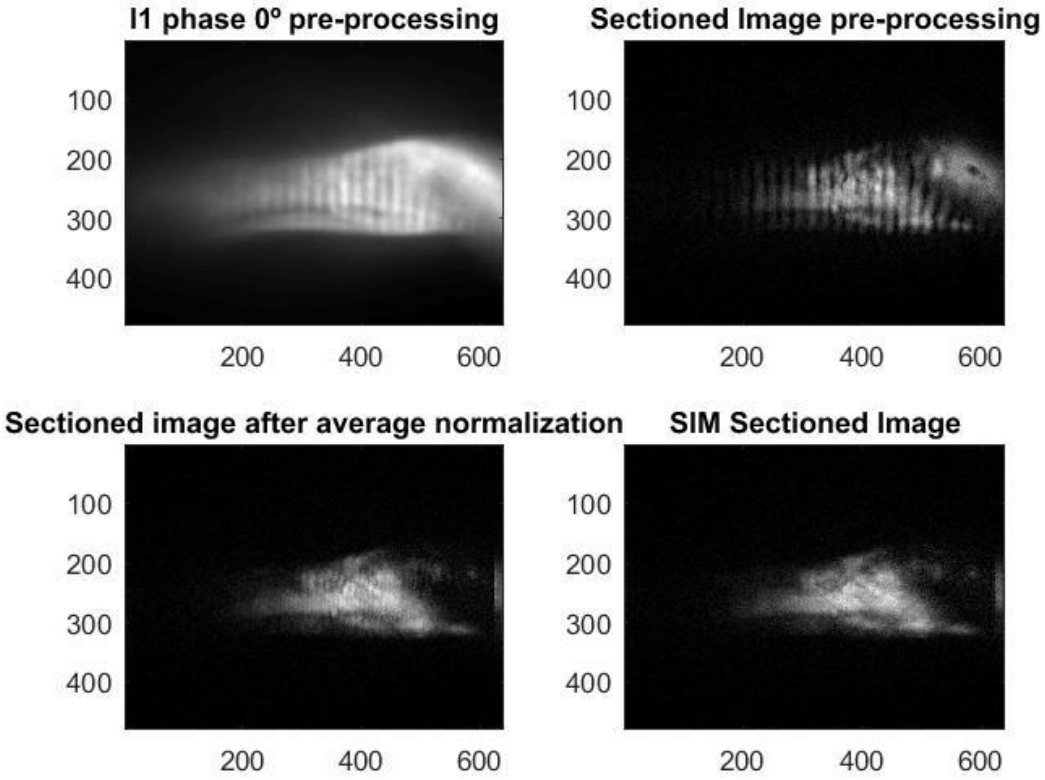

Figure 5.6 - On the top we have the structured (left) and sectioned (right) images of a sample of cotton fibres painted with fluorescent dye, without any processing. The images on the bottom are the sectioned image following the average normalization (left) and the final sectioned image (right).

5.2.1.3. Results analysis

In this analysis, we will not examine the results of the method over the pollen grains and cotton fibres separately, but as a whole.

The developed method was not able to fully eliminate the periodic pattern, since we can still observe small residues on parts of the final sectioned image. However, when we compare with the results without processing, the results in this matter can be regarded as satisfactory.

Individually, the moving average normalization is very effective, as the sectioned image following this step no longer contains the large pattern present on the initial image. The strips

that are still visible are much smaller, suggesting they correspond to higher order harmonics of the original pattern.

The notch filter is not as effective as the previous step, but is still capable of reducing the visible pattern in some areas of the images.

The other point of interest is the elimination of the out-of-focus portions from the image. Here the method appears to work well. In fact, when comparing the initial structured image and the resulting sectioned image on Figure 5.6, we can see that all the left side, where there was no pattern superimposed is successfully eliminated, while on the right side, only a very small portion of the out-ot-focus portion is present in the final image.

5.2.2. HiLo Microscopy

5.2.2.1. Pollen Grains

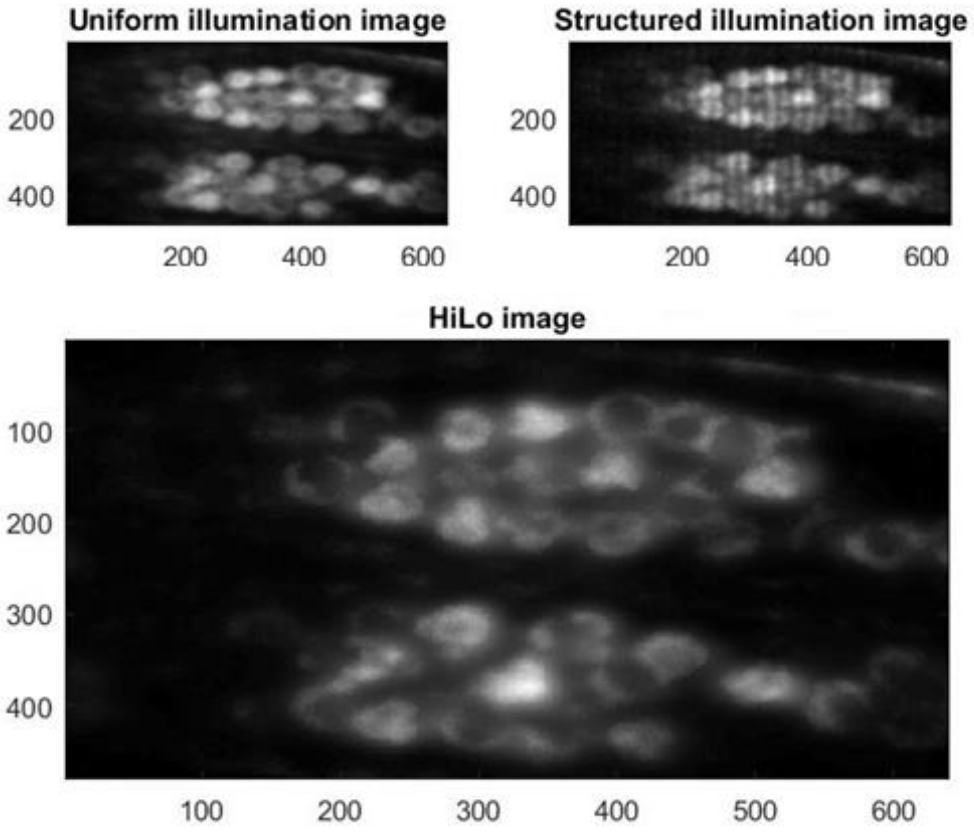

Figure 5.7 - On the top we have the unprocessed uniform (left) and structured (right) images from a pollen grain sample. On the bottom, we have the HiLo image.

5.2.2.2. Cotton Fibres

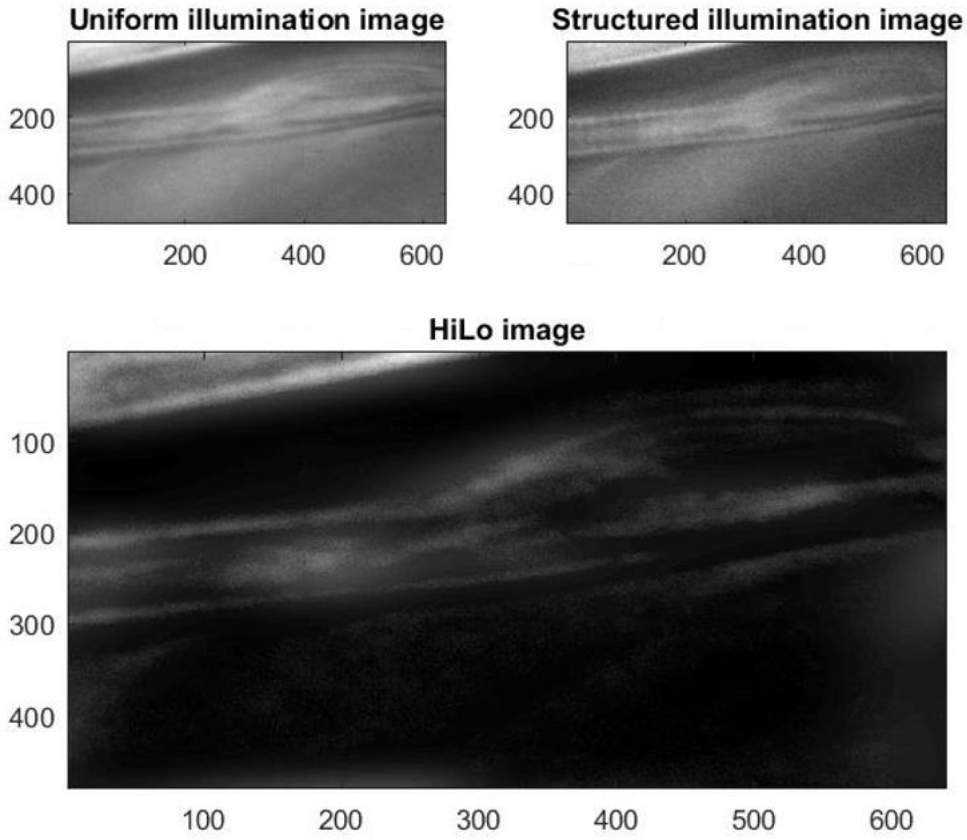

Figure 5.8 - On the top we have the unprocessed uniform (left) and structured (right) images from a sample containing cotton fibres painted with fluorescent dye. On the bottom, we have the HiLo image.

5.2.2.3. Results analysis

As mentioned, on HiLo microscopy only the final sectioned image can be evaluated.

This method seems to be extremely effective in what concerns the pattern suppression. In neither of the considered samples is visible any indication of the initial pattern that was used.

The background removal is not as successful. In fact, if we look to the images of the pollen grains, we can identify some regions where there is no pattern that are still visible on the sectioned image (see, for example, the right bottom corner).

5.3. Optical Sectioning Power of the Fluorescence Lifetime Microscope

In chapter 4 we have seen the theoretical approach to determine the expected axial resolution of the microscope. We have also seen how to measure the effective axial resolution. At this section, we present the corresponding results for both methods.

The tests were conducted using a physical grid with a frequency of 20 line pairs per millimetre (lp/mm).

The results expected according to theory are presented in Figure 5.9.

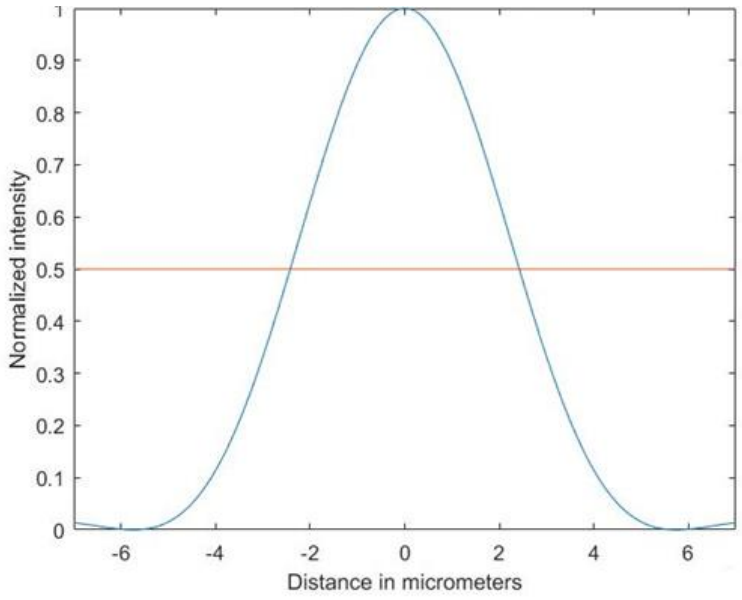

Figure 5.9 - Theoretical intensity decay with defocus.

In Figure 5.9, the blue line represents the intensity and the orange line is the line corresponding to half of the maximum. From the data on Figure 5.9, we conclude that the theoretical axial resolution of the microscope is 4.845 μm.

From the data, the theoretical axial resolution of the microscope is 4.845 μm.

Figure 5.10 represents the intensity measured at the fundamental frequency of the pattern, for each acquired image.

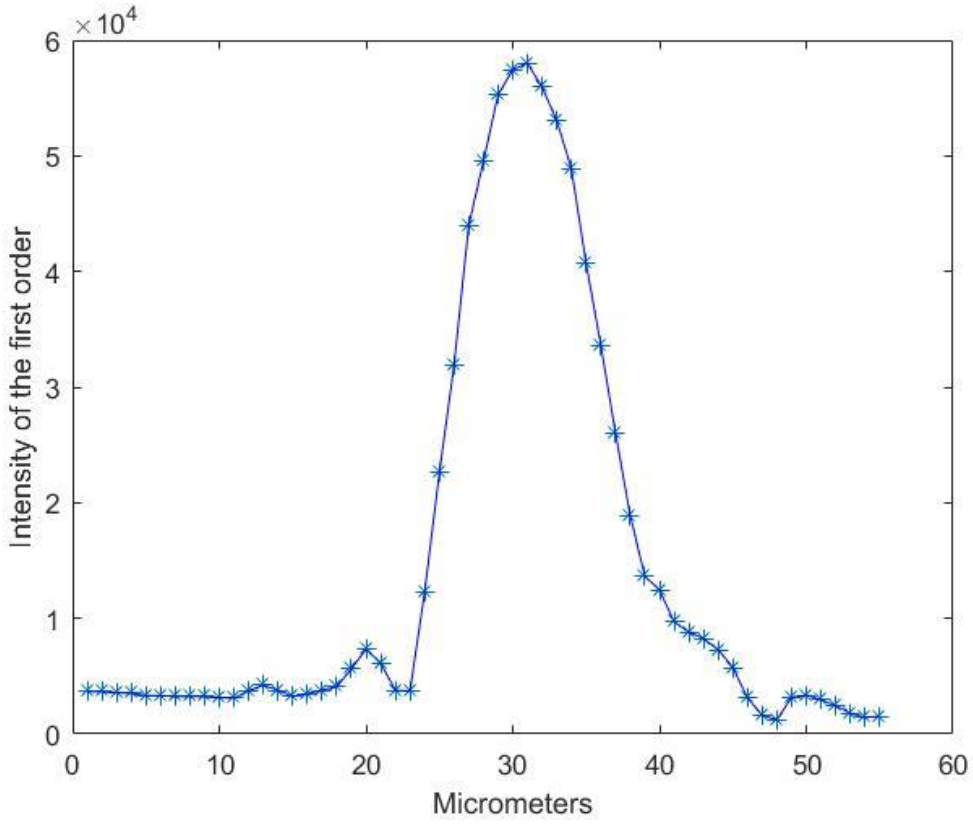

Figure 5.10 - Intensity at the pattern frequency.

To determine the axial resolution, the experimental data was fitted onto a Gaussian function. This process was done using the curve fitting tool in Matlab. The results are shown at Figure 5.11.

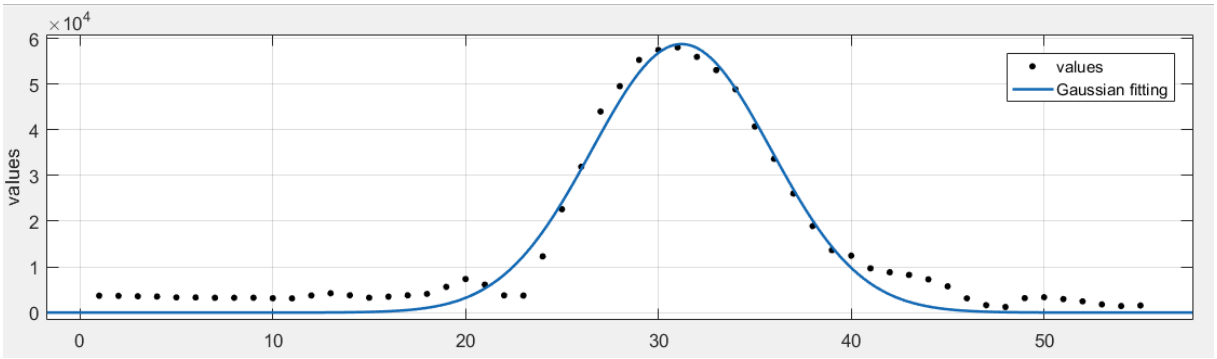

Figure 5.11 - Gaussian fitting of the data.

The fitting tool also estimates the coefficients of the Gaussian model with 95% confidence.

From definition, the FWHM is given by:

$$\boldsymbol{FWHM = 2\sqrt{2ln(2)} * \alpha} \quad (5.1)$$

As $C_1^2 = 2\ \alpha^2$, we obtain an axial resolution of (5.08 ± 0.40)μm. The uncertainty on the resolution value was obtained by error propagation.

The optical sectioning results for the two set-ups are present in table 5.1:

Table 5.1 - Theoretical and measured optical sectioning

Pattern Generation	**lp/mm**	**Theoretical Optical Sectioning (μm)**	**Measured Optical Sectioning (μm)**
Physical grid	20	4.84	5.08 ± 0.40
DMD	10.3	4.32	6.91 ± 0.45

Firstly, from the theoretical results, we can see that both set-ups should provide axial resolution under 5μm. Although those results are very satisfactory, it's the effective resolution that determines the resolving power of the microscope.

Starting with the physical grid, the measured resolution is in the range [4.68 ; 5,48] μm. The theoretical results are within that range, which means the system in this configuration is working well and the aberrations are minimal.

When it comes to the experimental set-up using the DMD, the results are not as good. Although an axial resolution of (6.91 ± 0.45) μm is not an inadequate result, the measured value is far off the expected optical sectioning.

This discrepancy can be caused by several factors. Assuming the DMD is perfectly calibrated, the first possibility is that the three converging lenses responsible for focusing the pattern on the back of the objective are introducing excessive aberration on the system. Please note that the set-up using a physical grid only has 2 two lenses between the grid and the sample. Another possible explanation is that the intensity of higher diffraction orders from the DMD is more substantial.

5.4. Fluorescence Lifetime Results

In this section, we will present the fluorescence lifetime map from a set of images processed with SIM and HiLo techniques on samples with pollen grains.

To be able to see the effect of the processing, the resulting fluorescence lifetime mapping of the sectioned images will be compared to the equivalent mapping from widefield images, using the same scaling.

5.4.1. Structured Illumination Microscopy

In this section the fluorescence lifetime obtained from processing a set of pollen grain images on Matlab and on FLIMfit are presented for SIM.

5.4.1.1. Lifetime Mapping

This chapter contains the fluorescence lifetimes of a widefield image without any processing and the resulting sectioned image.

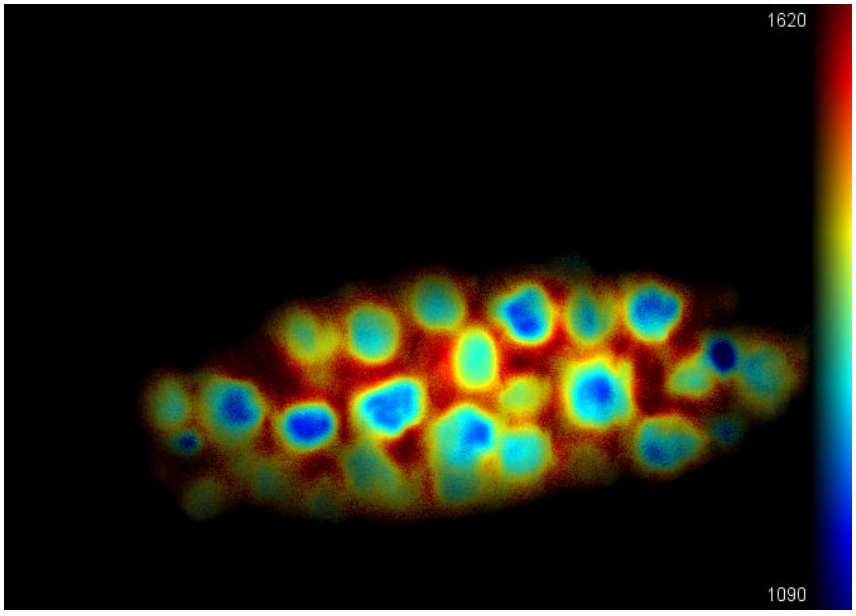

Figure 5.12 - Fluorescence lifetime mapping of the widefield image for SIM processing. The lifetime values are expressed in ps..

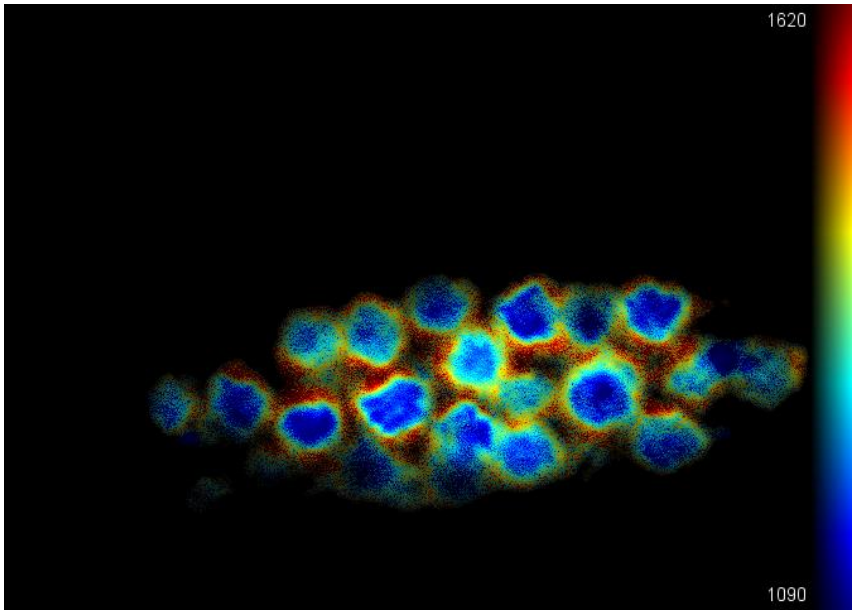

Figure 5.13 - Fluorescence lifetime mapping of the sectioned image for SIM processing. The lifetime values are expressed in ps.

5.4.1.2. Results analysis

The first observable difference on the images is that the widefield image shows longer lifetimes than the sectioned image. However, on the widefield, when observing the grains, we notice that the highest lifetimes are located between the grains whereas the lifetime values on the centre of some grains presents a bluish tone closer to the values of the sectioned image.

The most likely explanation is that on the widefield mapping there are components that mask the lifetimes by increasing them and with the optical sectioning we start to see the real fluorescence lifetime values of the pollen grain.

It is hard to evaluate the capacity to eliminate the out-of-focus contribution since we cannot know which grains had the projected pattern. Nevertheless, it is possible to see that some of the grains on the left bottom side of the sectioned image were eliminated and, that the unwanted contributions between the multiple grains are significantly reduced. However, it is still possible to observe regions with high lifetime values on the contour of the grains.

As a final note, the SIM processing time to analyse a set of 100 images on Matlab is 17 min and 20s. It is a long process, mostly due to the moving average normalization, which is a cycle with 277 248 pixels adjusted.

5.4.2. HiLo Microscopy

In this chapter are presented the resulting fluorescence lifetimes from the measurement of a pollen grain sample processed using the Matlab codes and the software FLIMfit. Finally, there will be an analysis of the results.

5.4.2.1. Lifetime Mapping

In this section are presented the fluorescence lifetime images of a widefield image without any processing and the resulting sectioned image.

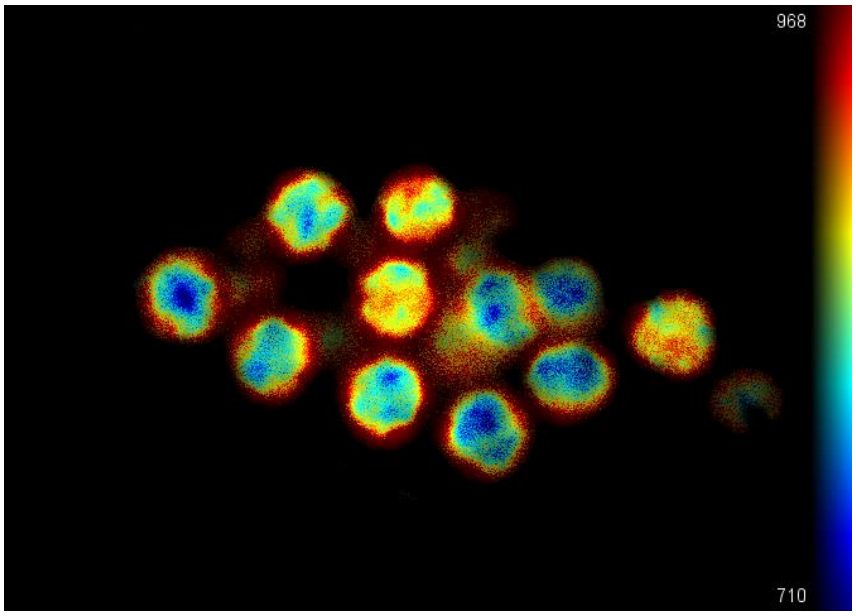

Figure 5.14 - Fluorescence lifetime mapping of the widefield image for HiLo processing. The lifetime values are expressed in ps.

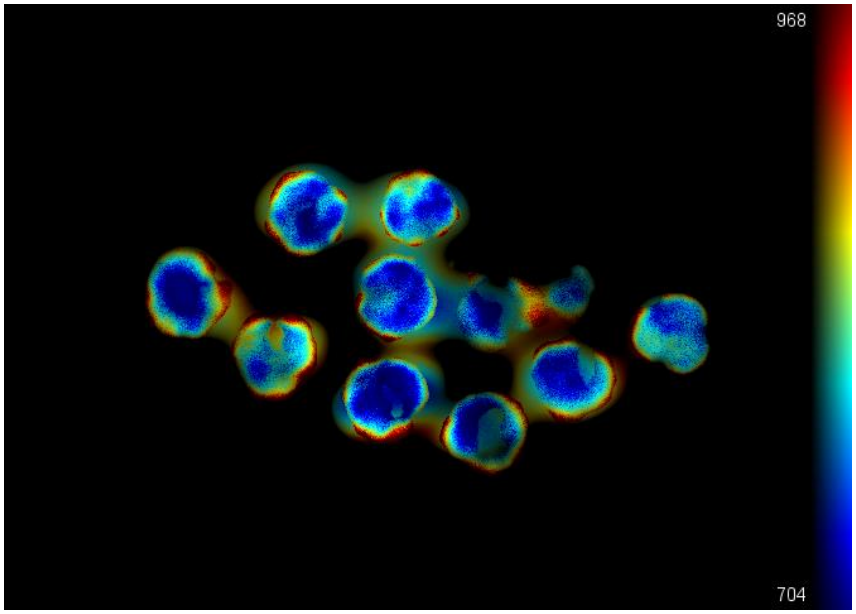

Figure 5.15 - Fluorescence lifetime mapping of the sectioned image for HiLo processing. The lifetime values are expressed in ps.

5.4.2.2. Results Analysis

On the HiLo lifetime maps we see a similar effect to one detected on the SIM method. The sectioned grains present a lower fluorescence lifetime in comparison to that measured in the uniform image, as indicated by their bluish centre.

The HiLo seems to cope really well with the residues between the grains and apparent out-of-focus grain, as it fully eliminates a partially visible grain on the right side of the uniform map. However, it appears to create an artefact in the form of a halo uniting some grains. The cause of this artefact is not clear as it has not been reported in any of analysed published papers regarding the HiLo method. It may be caused by an uneven transition between the Hi and Lo components used to create the sectioned image.

In terms of the processing time required to obtain a set of 100 sectioned image in Matlab, HiLo is extremely fast taking only 12s.

One noticeable difference between the presented results for SIM and HiLo processing concerns the fluorescence lifetime results. We obtained fluorescence lifetime lifetimes between 704 and 968 ps for HiLo, while for SIM the fluorescence lifetimes varied between 1090 and 1620 ps for SIM. That is due to the fitting methods used for both sets. On the SIM data processing, the

fitting was done without deconvoluting the Instrument Response Function (IRF) of the microscope. This function, measured by using a scattering solution as sample, can be seen as the impulse response of the microscope and has contributions from the finite duration of the light excitation pulse, the non-ideal gating profile and the finite bandwidth of the detector. Fitting without deconvoluting the IRF (i.e. fitting using a technique called Tail Fitting) always results in longer fluorescence lifetime values.

The HiLo measurements were done more recently, at a stage of the microscope development when its optical set-up was different from the one used to evaluate the SIM technique and the fitting procedures already included the deconvolution of the IRF curve. Therefore, the results from HiLo are probably closer to the true values.

6. CONCLUSIONS AND FUTURE WORK

The present project included the development of a Keplerian telescope to magnify the microscope light beam, as well as the development and the evaluation of two optical sectioning techniques, Structured Illumination Microscopy (SIM) and Hilo Microscopy (HiLo).

Regarding the Keplerian telescope design it is concluded that it has the required performance to fulfil its purpose. Using the optical simulation software Zemax OpticStudio, we concluded that the only significant aberration introduced by the telescope was spherical aberration, resulting in a maximum longitudinal displacement of 14μm. This value was considered acceptable. After introducing the Keplerian telescope in the optical set-up of the fluorescence lifetime microscope, the beam could fill the back of the objective without causing any noticeable degradation on the images.

Optical sectioning techniques aim to improve the axial resolution of widefield microscopy. Here the microscope presents very good results, having obtain during experimental tests an axial resolution of 5.08μm with a 20 lp/mm physical grid and 6.91μm using the DMD to generate the periodic pattern.

Overall, it was concluded that HiLo presented better results than SIM. Considering the analysis of individual images, they both showed relative success on the elimination of out-of-focus components. However, HiLo performed successfully in terms of supressing the pattern of the structured illumination, while images processed by SIM still retained residues of the initial pattern.

Concerning the fluorescence lifetime maps, both methods presented similar results. However, it is important to compare their processing times using Matlab. While HiLo would only require 12s to produce 100 sectioned images, SIM takes over 17 min to do the same task. This is clearly a big advantage for HiLo.

When analysing the fluorescence lifetime maps, we concluded that both methods cause a reduction of the observable fluorescence lifetimes on the sectioned maps, when compared to the values on the widefield maps, suggesting that both process are able to eliminate components that mask the real fluorescence lifetime of the sample.
For anyone taking on this project, improving the acquisition process would be a good starting point. Firstly, when a sequence of images for SIM is acquired, it is necessary to manually shift

the pattern on the software that controls the DMD. This process could be made automatic by creating a link between the DMD software and the acquisition software.

The acquisition software could also be associated with the processing methods developed in Matlab, so it would be possible to observe in real time the processed images. Still concerning the DaVis software, it would be useful if the program was able to automatically determine the delay at which the fluorescence intensity is highest.

Finally, the codes developed for this thesis could be improved, since neither method proved to be flawless. The SIM method was not able to fully supress the superimposed pattern and the HiLo method, when used to process a set of images to produce a fluorescence lifetime map, creates a small artefact on the resulting images.

REFERENCES

Bhattacharya, D., Singh, V. R., Zhi, C., So, P., Matsudaira, P., & Barbastathis, G. (2012, Dec 3). Three dimensional HiLo-based structured illumination for a digital scanned laser sheet microscopy (DSLM) in thick tissue imaging. *Optical Society of America*, pp. OPTICS EXPRESS 27337 - 27347.

Dupuis, G., Benabdallaha, N., Chopinauda, A., Mayeta, C., & Lévêque-Fort, S. (2013). Time-resolved wide-field optically sectioned fluorescence microscopy. *Three-Dimensional and Multidimensional Microscopy: Image Acquisition and Processing XX, Vol. 8589*, pp. 1 - 8.

FLIMfit. (n.d.). *http://docs.flimfit.org/*, (Accessed in June 2017).

Hecht, E. (2012). *Óptica.* Fundação Calouste Gulbenkian.

Heintzmann, R. (2006). Structured Illumination Methods. *Handbook of Biological Confocal Microscopy, Third Edition, edited by James B. Pawley, Springer Science+Business Media, LLC, New York*, 265-279.

Kubitscheck, U. (2013). *Fluorescence Microscopy: From Principles to Biological Applications.* Wiley-Blackwell.

Lakowicz, J. R. (Third Edition). *Principles of fluorescence spectroscopy.* Baltimore: Springer.

Lambert. (n.d.). *https://www.lambertinstruments.com/technologies-1/2014/12/4/fluorescence-lifetime-imaging-microscopy*, (Accessed in January 2017).

Marcu, L., French, P., & Elson, D. (2012). *Fluorescence lifetime spectrocopy and imaging.* Boca Raton: CRC Press.

Mertz, J., & Kim, J. (January/February 2010). Scanning light-sheet microscopy in the whole mouse brain with HiLo background rejection. *Journal of Biomedical Optics 15(1), 016027*, 1-7.

Microbial Life. (n.d.). *https://serc.carleton.edu/microbelife/research_methods/microscopy/fluromic.html*, (Accessed in January 2017).

Microscopy Resource Center. (n.d.). *http://www.olympusmicro.com/primer/techniques/confocal/confocalintro.html*, (Accessed in February 2017).

Microscopy Resource Center. (n.d.). *http://www.olympusmicro.com/primer/anatomy/mtfintro.html*, (Accessed in February 2017).

Microscopy U. (n.d.). *https://www.microscopyu.com/microscopy-basics/modulation-transfer-function*, (Accessed in February 2017).

Moleculcar Expressions. (n.d.). *http://micro.magnet.fsu.edu/primer/java/mtf/airydisksize/index.html*, (Accessed in February 2017).

Neil, M., Juskaitis, R., & Wilson, T. (1997). Method of obtaining optical sectioning by using structured light in a conventional microscope. *OPTICS LETTERS, 22*, 1905-1907.

Quadibloc. (n.d.). *http://www.quadibloc.com/science/opt0505.htm*, (Accessed in April 2017).

Richards, J. (1997). *Galilean and Keplerian Telescopes.* UW Departments Web Server - UNIVERSITY OF WASHINGTON: Site: History of Science Society.

Sauer, M., Hofkens, J., & Jorg, E. (2011). *Handbook of Fluorescence Spectroscopy and Imaging: From Ensemble to Single Molecules.* Wiley-vch.

Schaefer, L., Schaefer, J., & Schuster, D. (2004). Structured illumination microscopy: artefact analysis and reduction utilizing a parameter optimization approach. *Journal of Microscopy, Vol. 216*, 165-174.

Telescope Equations. (n.d.). *http://www.rocketmime.com/astronomy/Telescope/ResolvingPower.html*, (Accessed in February 2017).

Webb, S. E., Gu, Y., Lévêque-Fort, S., Siegel, J., Cole, M. J., Dowling, K., . . . Lever, M. J. (2002). A wide-field time-domain fluorescence lifetime imaging microscope with optical sectioning. *REVIEW OF SCIENTIFIC INSTRUMENTS*, 1898-1907.

ANNEX A

In this attachment is presented the integral code for the processing of SIM images developed in Matlab.

```
g1 = readimx('Name1.imx');
g2 = readimx('Name2.imx');
g3 = readimx('Name3.imx');

g1 = double(g1.Data);
g2 = double(g2.Data);
g3 = double(g3.Data);

g1 = g1';
g2 = g2';
g3 = g3';

%Definition of the masks size
step_i = 32;
step_j = 24;

%Moving average normalization
for i = 1:640 - step_i
    for j = 1:480 - step_j

        %step 1: Masks creation
        mask1(:,:) = g1(j : j + step_j-1,i : i + step_i-1);
        mask2(:,:) = g2(j : j + step_j-1,i : i + step_i-1);
        mask3(:,:) = g3(j : j + step_j-1,i : i + step_i-1);

        %step 2: Determination of the maximum
        averages(1) = mean(mean(mask1(:,:)));
        averages(2) = mean(mean(mask2(:,:)));
        averages(3) = mean(mean(mask3(:,:)));
        maximum = max(averages);

        %step 3: Replacing the central value
        g1(j + step_j/2 - 1, i + step_i/2 - 1) = g1(j + step_j/2 - 1, i +
          step_i/2 -1)*maximum/averages(1);
        g2(j + step_j/2 - 1, i + step_i/2 - 1) = g2(j + step_j/2 - 1, i +
          step_i/2 -1)*maximum/averages(2);
        g3(j + step_j/2 - 1, i + step_i/2 - 1) = g3(j + step_j/2 - 1, i +
          step_i/2 -1)*maximum/averages(3);

    end
end

%Definition of the sectioned image
Is = (3/sqrt(2)) * (((g1 - g2).^2 + (g1 - g3).^2 + (g2 - g3).^2) .^(1/2) );
```

```
%Definition of the widefield image
Ic = (g1 + g2 + g3)/3;

%Definition of the demodulation image
D = abs(Ic - g1);

%Collumn average of the demodulation image
mean_D = abs(fft2(mean(D,1)));

%Determination of the cutoff position
maximum = 0;
for j = 2:size(mean_D,2)/2
        if (mean_D(j) > mean_D(j-1) && mean_D(j) > mean_D(j-2) && mean_D(j)
         > maximum);
            cutoff = j;
            maximum = mean_D(j);
        end
end

%Definition of the positions where the Notch filter will be applied
peak(1) = 320 - 3*cutoff;
peak(2) = 320 - 2*cutoff;
peak(3) = 320 - cutoff;
peak(4) = 320 + cutoff;
peak(5) = 320 + 2*cutoff;
peak(6) = 320 + 3*cutoff;

%Fourier transform of Is
tf_Is = fftshift(fft2(Is));

%Aplication of the Notch filter
sigma = 100;
for i = 1:6
    H = Notch('gaussian', size(g1,1), size(g1,2), sigma, 240, peak(i), 1, 1,
     1);
    tf_Is = H.*tf_Is ;
end

%Final Sectioned image
Is = abs(ifft2(tf_Is));
```

ANNEX B

In this attachment is presented the HiLo code developed in Matlab.

```
In = readimx('Name1.IMX');
Iu = readimx('Name2.IMX');

%In = Structured image, Iu = Uniform image
In = double(In.Data);
Iu = double(Iu.Data);

In = In';
Iu = Iu';

%In normalization
Ratio = mean(mean(Iu))/mean(mean(In));

%Creation of the demodulation image
D=(Iu - Ratio.*In);

%To determine the cutoff frequency of the grid pattern
mean_D = abs(fft2(mean(D,1)));


%Determination of the cutoff frequency of the pattern
maximo = 0;
for j = 5:size(mean_D,2)/2
        if (mean_D(j) > mean_D(j-1) && mean_D(j) > mean_D(j-2) && mean_D(j)
          > maximo);
            cutoff = j;
            maximo = mean_D(j);
        end
end

%Fourier transform of D
Ft_D = fftshift(fft2(D));

%High pass of D with a cutoff frequency smaller than the fundamental frequency
sigma = 0.2 * cutoff;

%Filter definition
H = passa_banda('high','Gaussian',size(D,1) ,size(D,2), sigma);

%Filter aplication
Ft_D=H.*Ft_D;

D = abs(real(ifft2(dft_filt_gau)));

%Low pass of D with a Cutoff frequency slightly smaller than the fundamental
frequency
sigma=0.9*cutoff;
```

```
%Filter definition
H = passa_banda('low','Gaussian',size(D,1) ,size(D,2), sigma);

%Aplication of the filter
Ft_D = H .* Ft_D;

%Creation of the low frequency component
I_Lo=real(ifft2(Ft_D));

%To ensure there are no negative values
I_Lo(I_Lo<0) = 0;

%High pass of Iu with a Cutoff frequency complementar to the previous low
pass
Ft_Iu = fftshift (fft2(Iu));

%Definition of the filter
H =1 - H;

%Aplication of the filter
Ft_Iu=H .* Ft_Iu;

%Creation of the high frequency component
I_Hi =real(ifft2(Ft_Iu));

%To ensure there are no negative values
I_Hi(I_Hi<0) = 0;

Tf_Hi = fftshift(fft2(I_Hi));
Tf_Lo = fftshift(fft2(I_Lo));

%Creation of a small ring around the cutoff frequency
H = passa_banda('band', 'pass', 480, 640, round(cutoff-1), round(cutoff+1));

Tf_Hi = H.*Tf_Hi;
Tf_Lo = H.*Tf_Lo;

%Definition of the smoothing factor
n = sum(sum(abs(Tf_Hi)))/sum(sum(abs(Tf_Lo)));

%Creation of the HiLo image
IHiLo = n*I_Lo + I_Hi;
```